Ag-Au Alloy-Based Highly-Sensitive Plasmonic Sensor

by

Mohammad Ashfaqur Rahman Asif (200021201)

Fatema Tasnim Oyshi (200021206)

Safwan Sami (200021221)

A Thesis Submitted to the Academic Faculty in Partial Fulfillment of the Requirements for the Degree of

BACHELOR OF SCIENCE IN ELECTRICAL AND ELECTRONIC ENGINEERING

Department of Electrical and Electronic Engineering

Islamic University of Technology (IUT)
Gazipur, Bangladesh

October 2025

Ag-Au Alloy-Based Highly-Sensitive Plasmonic Sensor

Approved by:

Sagor

Dr. Rakibul Hasan Sagor
Supervisor and Professor,
Department of Electrical and Electronic Engineering,
Islamic University of Technology (IUT), Boardbazar, Gazipur-1704.

Date: 20 OCT 2025

Declaration of Authorship

This is to certify that the work presented in this thesis paper is the outcome of research carried out by the candidates under the supervision of Dr. Rakibul Hasan Sagor, Professor at the Department of Electrical and Electronic Engineering (EEE), Islamic University of Technology (IUT).

Authors

Mohammad Ashfaqur Rahman Asif	Fatema Tasnim Oyshi	Safwan Sami
ID: 200021201	ID: 200021206	ID: 200021221

Contents

List of Tables

List of Figures

List of Acronyms

Ag	Silver
Au	Gold
AZO	Aluminum-doped Zinc Oxide
CMOS	Complementary Metal-Oxide-Semiconductor
COMSOL	COMSOL Multiphysics (Simulation Software)
FEM	Finite Element Method
FDTD	Finite-Difference Time-Domain
FOM	Figure of Merit
FWHM	Full Width at Half Maximum
GaAs	Gallium Arsenide
GZO	Gallium-doped Zinc Oxide
HfO_2	Hafnium Oxide
ITO	Indium Tin Oxide
LOD	Limit of Detection
LOC	Lab-on-a-Chip
LSPR	Localized Surface Plasmon Resonance
MIM	Metal–Insulator–Metal
PML	Perfectly Matched Layer
Q-factor	Quality Factor
RI	Refractive Index
RIU	Refractive Index Unit
SAM	Self-Assembled Monolayer
SDG	Sustainable Development Goal
Si	Silicon
SNR	Signal-to-Noise Ratio
SPP	Surface Plasmon Polariton
SPR	Surface Plasmon Resonance
SSMO	Sudanese Standards and Metrology Organization
Ta_2O_5	Tantalum Pentoxide
TCO	Transparent Conducting Oxide
TiN	Titanium Nitride
TM	Transverse Magnetic
ZrN	Zirconium Nitride

Acknowledgements

First and foremost, we want to thank Allah for giving us the strength, patience, and willpower to finish this thesis.

We would like to thank Prof. Dr. Rakibul Hasan Sagor from the bottom of our hearts for his invaluable guidance, helpful feedback, and constant support during this research. His advice has always motivated us and has been a key factor in determining the direction and quality of our work.

We are also very grateful to Mr. Sheikh Montasir Mahbub and Mr. A. K. M. Rakib for their early guidance and lessons, which gave us the basic knowledge and motivation we needed to start this project. We also want to thank all the teachers in the Department of Electrical and Electronic Engineering at the Islamic University of Technology (IUT) for always being there for us, giving us advice, and cheering us on during our studies.

Finally, we want to thank our families from the bottom of our hearts for their unconditional love, endless patience, and unwavering faith in us. Their constant support and encouragement have been the most important things that have kept us going and helped us succeed.

Mohammad Ashfaqur Rahman Asif
Fatema Tasnim Oyshi
Safwan Sami
October, 2025

Abstract

The proposed refractive index sensor has an alloy-insulator-alloy construction. Au-Ag alloy provides several advantages over pure metal in terms of chemical stability, performance and fabricability. The material under the sensing unit features interdigitated finger-like structures with a metallic nanorod inserted into it. When air is used as an insulator in conjunction with an alloy, our sensor has demonstrated better performance than with pure metal. It has attained a sensitivity of 3730 nm/RIU and FOM of 9.29 for 50%-50% Au-Ag concentration. Later, we have used $Ta_2 0_5$ as the dielectric medium since it has a higher bandgap and a high refractive index, paving the way for stronger mode confinement. That's why we have replaced the air medium with $Ta_2 0_5$ in our final structure. Eventually, with a suitable metallic alloy composition, our sensor exhibits a maximum sensitivity and FOM of 4750 nm/RIU and 29.83, respectively. Furthermore, the wide operating region of the RI sensor helps to encompass multiple applications. We have utilized our proposed structure to efficiently measure blood concentration. It can also specifically determine hemoglobin concentration with minimal error percentage. Besides that, edible oil can easily be classified based on the resonant wavelength shift. Overall, the unique sensor structure, when employed with alternative materials, demonstrates exceptional performance and versatile applicability.

Chapter 1

Introduction

Recently, nanoscale devices utilizing surface plasmon polaritons (SPPs) have attracted significant interest due to their ability to confine and guide light at dimensions smaller than the wavelength of illumination. [1] [2]. SPPs are localized electromagnetic waves that decay exponentially as they move at the boundary between a dielectric material and a conductive medium with a high concentration of free carriers [3]. SPPs have more momentum compared to free-space light of the same frequency, which is why their electromagnetic field is tightly confined to the metal-dielectric interface [4]. The downscaling of the optical devices was temporarily stopped because of the diffraction limit. However, SPPs can overcome this diffraction limit [5], and further miniaturization of plasmonic sensors is possible.

In order to control these tightly bound electromagnetic fields, different kinds of plasmonic waveguides (WGs) have been used. These types include ridge, hybrid, and slit-type configurations. Among these, the metal–insulator–metal (MIM) configuration is the most popular due to its small mode size [6], its ability to keep the field confined [7], and its good balance between propagation length and ohmic losses [8]. All these characteristics make the MIM waveguide a suitable candidate for refractive index (RI) sensors. Many RI sensors have been proposed with different types of MIM waveguides and different types of resonators. These include RI sensors with elliptical resonators with a sensitivity of 1000 nm/RIU, semicircular resonators with a sensitivity of 2900 nm/RIU [9], asymmetric MIM waveguides with a sensitivity of 1114 nm/RIU [10], and nanorod array resonators with 1090 nm/RIU [11].

Plasmonic refractive index (RI) sensors allow real-time detection of biomolecular interactions by taking advantage of the high sensitivity of surface plasmon resonance (SPR) or localized surface plasmon resonance (LSPR) to very small changes in the dielectric environment near a metal-dielectric interface [12]. Gold (Au) and silver (Ag) are standard plasmonic metals in such systems. Although Ag usually offers sharper resonances and lower loss in the visible regime, but is chemically less stable; Au offers chemical stability and thermal stability. But it has a broader resonant line width and reduces sensitivity [13] [14] [15]

Tantalum pentoxide is recently being introduced in plasmonic sensors due to its high refractive index, large energy band gap, and high temperature resistance and tunability [16] [17] [18]. In recent years, integration of tantalum pentoxide with gold and silver has shown better results [16] [17].

In order to overcome the problems of the mono-metallic RI sensors and to gain the advantages of both gold and silver, we proposed a structure based on an Ag-Au alloy integrated with a tantalum pentoxide waveguide. Our proposed sensor shows a maximum sensitivity of 1000 nm/RIU and FOM (figure of merit) of 20. Our sensor shows potential to be used in biosensing, as it can detect from the visible light range to the mid-IR range. We used this sensor to find the specific gravity and hemoglobin concentration of blood while differentiating between different oils.

1.1 Plasmonics

Plasmonics studies how light interacts with collective electron oscillations at metal-dielectric interfaces. This creates surface-bound modes that compress optical energy far below the diffraction limit and greatly increase the interactions between light and matter [19] [20] [21]. In this image, two processes are used for sensing: propagating surface plasmon polaritons (SPPs) on thin films and localized surface plasmon resonances (LSPRs) on nanoparticles or nanostructures. Both create strong, near-field hotspots that can make small changes in the refractive index or molecular binding events that can be measured in real time without labels [20] [22] [23] [24]. The plasmonic near field usually only goes a few hundred nanometers into the analyte, so the transducer is naturally surface-selective, which is the same scale as functional monolayers, biomolecular layers, and interfacial chemistry used for specificity [22] [23] [24].

One of the main goals of designing plasmonic sensors is to get the most signal per refractive index unit while reducing noise and drift. In practice, this means making sharp spectral features and high quality factors to improve the slope at the operating point and the ultimate limit of detection [23] [25] [26]. Nanoparticle arrays that support surface lattice resonances (via diffractive coupling) and metasurfaces that host Fano interferences (via bright–dark mode coupling) both narrow the linewidth and steepen dispersion, turning tiny index changes into resolvable spectral shifts with improved figures of merit [25] [26]. Gold and silver are still the best materials for the visible and near-IR because they have good dielectric functions. However, other materials like titanium nitride, aluminum (for UV), transparent conducting oxides, doped semiconductors, and even graphene can increase the spectral range, add electrical tunability, and lower costs or make them more thermally stable. However, ohmic loss will always limit Q and propagation length [27] [28] [29] [30].

Plasmonics is moving from benchtop prisms to chip-scale systems because of trends in integration. Long-range SPP waveguides increase the length of interactions for inline sensing with low scattering. Metal–insulator–metal slots and cavities, on the other hand, provide extreme confinement for ultracompact, high-contrast resonances that work well with microfluidics and multiplexed readouts [31] [32]. In practical terms, a modern plasmonic sensor is a stack of decisions about the mode type (SPP/LSPR/SLR), geometry (film, particle, slot, cavity, lattice), and material (Au/Ag or alternatives) that are made based on the size of the analyte, the operating band, and the target detection limit. When these choices are made coherently, plasmonics provides fast, label-free, and highly sensitive transduction that is perfect for chemical and biosensing at the nanoscale [24] [25] [29] [31] [32] [33].

1.2 Surface Plasmon Polaritons

Surface plasmon polaritons (SPPs) are electromagnetic waves that propagate along the metal–dielectric boundary. They arise from the coupling between incident light and the collective oscillations of free electrons within the metal [38]. These are surface-confined waves that travel parallel to the interface is formed at the metal surface by coherent electron charge density waves (plasmons) driven by the oscillating electromagnetic field of light. Ritchie was the first to notice this phenomenon in the 1950s, and his pioneering study established that these surface modes occurred on metal films [38]. SPPs have sparked a lot of interest in physics, chemistry, and materials science because of advances in nanofabrication, which now allow for precise control of metal nanostructures and, as a result, SPP behavior [34] [35].

One of the unique features of SPPs is their ability to confine light beyond the diffraction limit and compress optical energy into subwavelength dimensions at the metal-dielectric interface [35]. This subwavelength confinement and the strong local fields of SPPs enable a wide variety of nanoscale photonic devices and enhanced sensing techniques [36]. For example, SPP-based refractive index sensors can achieve extremely high sensitivity, making them ideal for detecting even the smallest changes in biological or environmental samples [42], [50]. Similarly, SPPs are employed in many integrated nanophotonic components to control light at the nanoscale—such as filters, switches, demultiplexers, couplers, and splitters [43] [46]. These devices accomplish things that conventional diffraction-limited optics cannot by utilizing the strong light-matter interaction of SPPs [35] [36]. These advancements in SPP-based components have enormous potential for use in data processing, lab-on-a-chip sensing, telecommunications, and other fields [47] [48].

Many sensing applications take advantage of SPPs' high sensitivity to variations in the refractive index of the nearby dielectric [49]. The propagation constant and resonance condition of the SPP are changed by a slight change in the surrounding medium, such as that caused by molecules binding to the metal surface [41]. Techniques like surface plasmon resonance (SPR) sensing and surface-enhanced Raman scattering, which use changes in resonance wavelength or increased signal intensity to detect the presence of analytes, are supported by this sensitivity [39] [40]. To sum up, surface plasmon polaritons offer a special way to confine and direct light at the nanoscale, setting the stage for plasmonic devices that can do far more than conventional photonic systems [34] [36].

1.3 Plasmonic Waveguide Topologies

Unlike traditional dielectric waveguides, which use total internal reflection for confinement, plasmonic waveguides are nanoscale guiding structures that use SPPs to channel light [35]. Plasmonic waveguides achieve mode sizes well below the free-space wavelength by directing light along metal-dielectric interfaces instead of inside a bulk dielectric [36]. The two main plasmonic waveguide configurations—metal–insulator–metal (MIM) and insulator–metal–insulator (IMI)—are introduced in this section. Each offers unique confinement and propagation trade-offs [44].

In the Metal–Insulator–Metal (MIM) waveguide, a thin dielectric core is sandwiched between two metal claddings, forming a nanoscale slot that supports tightly confined SPP modes [44] [45]. The electromagnetic field is largely concentrated in the dielectric gap while bound to the metal surfaces on both sides [46]. This configuration affords extremely strong mode confinement and intense field enhancement within the gap, which is highly advantageous for sensing applications that require light–matter interaction in a small volume [45] [50]. Additionally, the MIM structure allows for straightforward planar fabrication and supports effective interference of multiple SPP modes, enabling complex plasmonic circuits [42] [44]. However, the tight confinement comes at the cost of higher propagation loss due to metal absorption—the energy of the SPP attenuates over a relatively short distance as it travels along the waveguide [35] [36]. The propagation length of MIM modes is therefore limited, on the order of a few tens of microns or less, which is a reasonable trade-off for many on-chip nanophotonic systems that prioritize footprint over long-distance transmission [51].

In contrast, the Insulator–Metal–Insulator (IMI) waveguide consists of a metal layer embedded between two dielectric layers [46]. Here, the SPP mode extends along the outer surfaces of the thin metal film and can penetrate farther into the surrounding dielectrics, resulting in a longer propagation range compared to MIM [45]. These IMI configurations support long-range SPPs that can travel greater distances owing to lower attenuation per unit length [35]. However, the IMI waveguide faces weaker field confinement—since the mode is more distributed in the dielectrics and less tightly bound to the metal interface, the local field intensity near the metal is reduced [35] [44]. This reduced confinement in IMI topologies means the interaction of the mode with any sensing target or active material at the interface is less enhanced, potentially limiting device sensitivity [41] [46].

MIM waveguides are still the best option for plasmonic refractive index sensors and other nanophotonic devices requiring strong field localization, even though IMI modes have a longer range [42] [46]. Since even slight variations in the dielectric gap greatly disturb the tightly confined SPP mode, MIM designs' capacity to confine electromagnetic energy into minuscule volumes results in an increase in sensitivity for the detection of changes in the refractive index [43] [51]. Additionally, better material and fabrication selections keep reducing propagation losses, guaranteeing high signal integrity for sensing applications [44] [47]. In conclusion, the MIM topology is ideal for integrated plasmonic devices due to its excellent field confinement and controllable loss [48].

1.4 Basic Functionalities of an RI Sensor

A refractive index (RI) sensor operates on the principle that any variation in the refractive index of a medium in proximity to an optical field modifies the propagation characteristics of that field, resulting in a measurable optical signal. These sensors are designed to convert a minute change in the refractive index (Δn) into a corresponding change in an optical parameter such as wavelength, angle, phase, or intensity. The fundamental concept is based on the interaction between light and the surrounding medium at an interface, typically through an exponentially decaying near-field that extends into the sensing region [52].

In any surface plasmon resonance (SPR) or localized surface plasmon resonance (LSPR) configuration, the resonance condition depends on the effective refractive index at the dielectric–metal interface. Upon the introduction of analyte molecules, the local refractive index in the vicinity of the interface changes, resulting in a corresponding change in the resonance wavelength ($\Delta\lambda$) or resonance angle ($\Delta\theta$) [53]. The change in resonance wavelength is linearly proportional to the refractive index change and can be expressed as

$$S_\lambda = \frac{\Delta\lambda}{\Delta n} \tag{1.1}$$

where S_λ denotes the sensitivity of the sensor. High-sensitivity plasmonic nanostructures, such as some metal–insulator–metal (MIM) cavities or periodic nanoparticle arrays, can generate strongly confined electromagnetic fields and nonlinear optical (NLO) responses, thereby enhancing the overall sensitivity of the system [54]. Consequently, the effective sensitivity range of RI sensors is limited to the penetration depth of evanescent fields, which is typically a few hundred nanometers from the interface. This nature makes RI sensors intrinsically surface-sensitive and can be used advantageously to investigate thin molecular layers, biomolecular interactions, or surface adsorption phenomena [55]. This sensor is, however, not selective because of the IR response of the sensor to any change in refractive index at or near a surface. For chemical or biochemical specificity, the sensing surface is designed to incorporate recognition molecules. For example, self-assembled monolayers (SAMs), antibodies, aptamers, or molecularly imprinted polymers. The detection signal is a localized change in refractive index caused by the selective binding of these functional layers to target molecules [56].

The performance of a refractive index (RI) sensor is commonly characterized by its sensitivity, resolution, and figure of merit (FOM). The *resolution* represents the smallest change in refractive index that can be accurately detected, whereas the *sensitivity* indicates how strongly the sensor responds to a change in the refractive index. The limit of detection (LOD) is estimated as

$$\text{LOD} = \frac{3\sigma}{S_\lambda} \tag{1.2}$$

where σ is the standard deviation of the baseline noise and S is the sensor sensitivity. Also,

$$\text{FOM} = \frac{S_\lambda}{\text{FWHM}} \tag{1.3}$$

A narrower resonance peak (i.e., a higher quality factor, Q) enhances detection precision by enabling the resolution of smaller spectral shifts [57]

Since the metal/dielectric constants and the surrounding medium's refractive index are both temperature dependent, temperature variation is one of the main problems with RI sensing. Temperature-compensated calibration models, dual-wavelength interrogation, or differential referencing techniques are used to reduce such errors [58]. Dual-parameter systems can measure temperature and refractive index simultaneously in sophisticated sensor designs to separate their effects on the sensing signal [59].

Both optical and kinetic factors influence an RI sensor's dynamic response. Mass transport and molecular binding kinetics limit the system response, but the optical response to a change in refractive index is nearly instantaneous. By interfering with the binding process, the surface can be renewed in biosensing, enabling the reuse of the same sensor chip [60].

There are several ways to interrogate RI sensors. Phase interrogation detects changes in phase between reference and sensing beams, angular interrogation tracks changes in the reflectivity angle, and spectral interrogation uses a broadband source to measure the resonance wavelength shift. Every approach has a trade-off. While intensity-based techniques allow for simpler and more compact sensor systems, spectral and phase interrogation typically offer higher sensitivity [61].

An RI sensor's primary function is to use resonance to transform changes in refractive index into optical signals that can be detected. Field confinement, resonance sharpness and stability are all necessary for its operation. Plasmonic nanostructures, which promise ultra-compact, real-time, and label-free detection capabilities, are being used in recent research efforts to improve the performance parameters of RI sensors [62].

1.5 Thesis Objective

The primary objective of this thesis is to design and optimize a highly sensitive plasmonic refractive index sensor by addressing the limitations of conventional plasmonic materials and waveguide structures [50]. In particular, this research aims to leverage material and structural innovations to enhance sensor performance beyond what is achievable with standard gold- or silver-based devices [48]. The specific objectives are as follows:

1. Review conventional plasmonic materials (gold and silver) and their limitations regarding optical losses and chemical stability.

2. Investigate hybrid or alternative plasmonic material strategies, such as Ag–Au alloys, to improve sensitivity, tunability, and longevity.

3. Develop theoretical models and perform finite element simulations to analyze surface plasmon polariton (SPP) propagation and resonance in the proposed structures.

4. Design and optimize a modified metal–insulator–metal (MIM) waveguide sensor, adjusting geometrical parameters to achieve higher sensitivity, narrower resonance, and an improved figure of merit (FOM).

5. Demonstrate practical applications of the sensor in detecting refractive index variations in gases, biological samples, and liquids, showcasing its real-world feasibility.

Through these objectives, the thesis aims to contribute a novel plasmonic sensor design that advances performance metrics via both material and structural innovation.

Chapter 2

Literature Review

2.1 Evolve of RI Sensor in Recent Years

The development of refractive index (RI) sensors based on plasmonic structures has attracted significant research interest due to its potential for highly sensitive detection in chemical and biological sensing applications. The following Table summarizes recent work on various RI sensor designs, highlighting their structural configurations, sensitivity, figure of merit (FOM), and year of publication. This comparative overview provides information on the evolution of performance and optimization strategies employed in recent sensor technologies.

Table 2.1: Comparative overview of recent RI sensors

RI Sensor Design	**Sensitivity (nm/RIU)**	**FOM** $(\mathbf{RIU})^{-1}$	**Year**	**Ref**
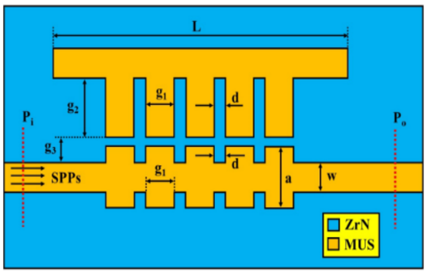	1445.46	140.96	2023	[63]
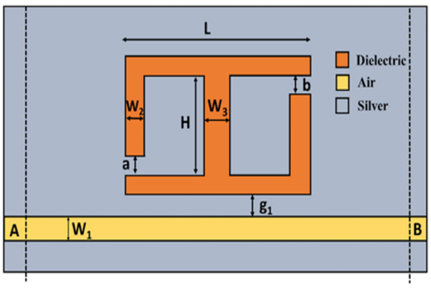	2963.73	25.1	2023	[64]
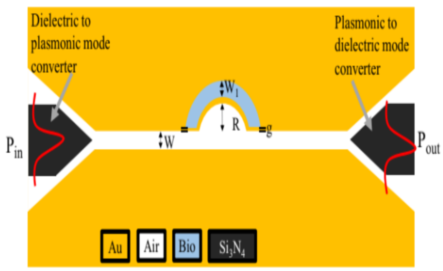	941.33	-	2023	[65]

RI Sensor Design	Sensitivity (nm/RIU)	FOM $(\mathrm{RIU})^{-1}$	Year	Ref
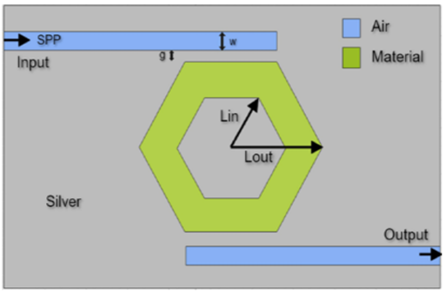	2950	40.055	2023	[66]
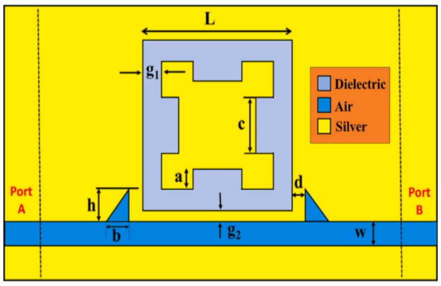	3270.3	31.154	2023	[67]
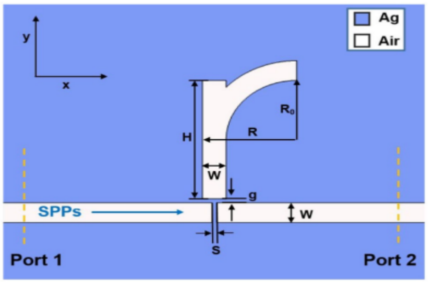	1333	5876	2022	[68]
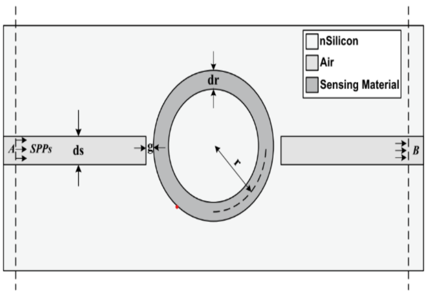	4900	-	2022	[69]
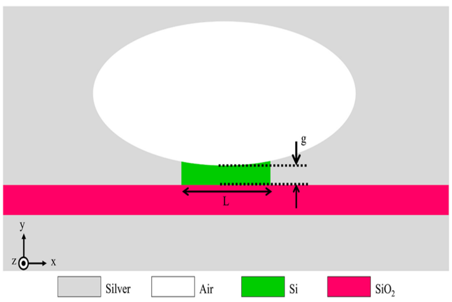	550	282.5	2021	[70]

RI Sensor Design	Sensitivity (nm/RIU)	FOM $(\mathrm{RIU})^{-1}$	Year	Ref
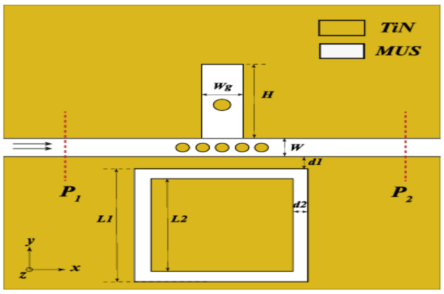	1074.88	32.4	2021	[71]
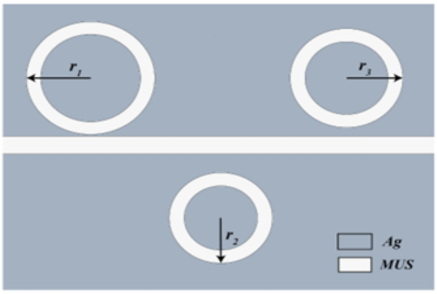	3573.3	21.9	2021	[72]
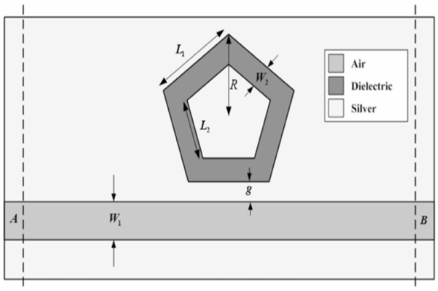	2325	46	2021	[73]
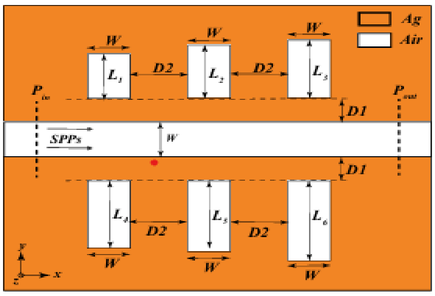	865.31	218.8	2021	[74]

Recently, refractive index (RI) sensors based on plasmonic and metal–insulator–metal (MIM) structures have received extensive attention due to their strong field confinement, high sensitivity, and potential for integration into lab-on-chip devices. Early studies from 2021 focused on improving structural geometries and exploring alternative plasmonic materials to overcome the intrinsic losses of noble metals. For instance, Khani and Hayati [70] proposed an elliptical resonator coupled with a MIM waveguide, achieving ultra-high sensitivity through enhanced Fano resonance effects. Similarly, Yaseer et al. [74] developed a color-optimized plasmonic sensor, emphasizing spectral tunability for colorimetric applications. Around the same period, Rashid et al. [72] introduced a multi-ring structured nanosensor for gas sensing and biomaterial detection, while Mahmud et al. [73] designed a ring-type pentagonal resonator yielding high sensitivity. Furthermore, Tathfif et al. [71] demonstrated the use of titanium nitride (TiN) as an alternative plasmonic material, offering CMOS compatibility and reduced optical losses.

By 2022, the research emphasis shifted toward novel resonator geometries and semiconductor based plasmonic structures for improved performance. Rohimah et al. [68] investigated an R-shaped resonator integrated into a MIM waveguide, exhibiting Fano resonance behavior with enhanced figure of merit (FOM). Faruque et al. [69] introduced a doped silicon-based plasmonic sensor, serving as an efficient alternative to traditional MIM designs, combining high sensitivity with fabrication simplicity. These developments indicated a move toward material innovation and spectral selectivity in RI sensing.

The recent advancements (2023) have focused on complex hybrid and CMOS compatible plasmonic configurations, enhancing both tunability and integration potential. Rakib et al. [63] presented a zirconium nitride (ZrN)-based plasmonic sensor, demonstrating tunable optical properties and compatibility with standard semiconductor processes. Rahad et al. [64] expanded on biomedical applications by employing plasmonic sensing for biomarker detection relevant to diseases such as diabetes, anemia, and cancer. Butt et al. [65] explored a metal–insulator–metal waveguide system with optimized sensitivity and spectral response. Additionally, Afdol et al. [66] designed an asymmetric hexagonal plasmonic sensor integrating MIM and Si–insulator–Si configurations, achieving enhanced sensitivity through strong coupling effects. Rahad et al. [67] further demonstrated the versatility of plasmonic RI sensors in fuel classification and adulteration detection, showcasing their adaptability across industrial and biomedical domains.

Overall, the evolution of RI sensor research reveals a clear trajectory from basic MIM resonator designs toward multifunctional, CMOS-compatible, and material-diverse sensors. These advancements emphasize the growing potential of plasmonic RI sensors for next-generation optical sensing, diagnostics, and environmental monitoring applications.

2.2 Use of Alternative Materials

Conventional plasmonic sensors typically employ noble metals like gold (Au) and silver (Ag) for their strong SPR properties; however, their use is limited by high cost, poor thermal stability, and considerable optical losses in the visible spectrum. Therefore, researchers have been investigating *alternative plasmonic materials* that are more stable, tunable, and compatible with microelectronics fabrication processes [75].[76]

Transition metal nitrides such as titanium nitride (TiN) and zirconium nitride (ZrN) are among the most promising alternatives. These nitrides exhibit metallic optical behavior, high melting points, and excellent thermal and chemical stability. TiN and ZrN have plasmonic responses in the visible and near-infrared ranges, and unlike noble metals, they can be grown using standard CMOS processes [77] [78]. Recent studies have demonstrated the use of TiN and ZrN for refractive index sensing, showing comparable sensitivity to gold-based designs while maintaining superior mechanical durability [77].

Transparent conducting oxides (TCOs) such as ITO, AZO, and GZO can function as plasmonic materials when heavily doped, with tunable carrier concentrations that enable shifting the plasmonic resonance into the near-infrared (NIR) region.[77] [79]. TCOs are advantageous for sensors operating in biological windows, where light absorption by tissues and water is minimal. They also exhibit lower losses than noble metals in the infrared region, which improves the overall figure of merit of sensors [77] [80].

Dielectric oxides such as hafnium oxide (HfO_2), titanium dioxide (TiO_2), and aluminum oxide (Al_2O_3) have also been studied for plasmonic structures. These dielectrics can enhance field confinement and reduce energy losses when combined with plasmonic materials [80] [81]. For instance, TiO_2 is often used as a high-index dielectric spacer in metal–insulator–metal (MIM) configurations, leading to sharper resonance peaks and improved sensor performance. Similarly, HfO_2 has been used to improve thermal and chemical stability in multilayer plasmonic devices, maintaining consistent sensitivity in harsh environments [81].

Beyond nitrides and oxides, **doped semiconductors** such as indium oxide and doped silicon have been used as plasmonic materials in the infrared region. Their plasma frequencies can be controlled by doping, making them tunable and integrable with existing electronic circuits [77] [82]. Additionally, **two-dimensional (2D) materials**, like graphene, exhibit highly confined and tunable plasmonic modes in the mid-infrared to terahertz ranges, allowing dynamic sensing and miniaturized device designs [83] [84].

In summary, alternative materials like nitrides, oxides, and doped semiconductors offer versatile options for developing high-performance plasmonic sensors. These materials overcome the limitations of noble metals by offering better tunability, environmental stability, and fabrication compatibility, paving the way for next-generation plasmonic sensing platforms across visible, near-infrared, and mid-infrared ranges [75] [77].

Chapter 3

Methodology

3.1 Wave Theory and Maxwell's Equations

3.1.1 Wave Theory

Wave theory explains how energy moves through space or a medium without the permanent movement of matter. A wave is basically a disturbance that travels from one point to another, carrying energy and information. There are many kinds of waves, such as sound waves, water waves, and electromagnetic waves. In an electromagnetic wave, the vibration of the electric field and magnetic field repeats in space and time, creating an oscillating pattern. A simple mathematical form of a wave can be written as

$$\Psi(x,t) = A\sin(kx - \omega t + \phi) \tag{3.1}$$

here A is the amplitude, k is the wave number, ω is the angular frequency, and ϕ is the phase. This equation describes how the wave varies with both position (x) and time (t). The relation between speed, frequency(f) and wavelength(λ) is given below

$$v = f\lambda \tag{3.2}$$

3.1.2 Wave Equation

It is a mathematical expression that shows how waves move through space and time, which connects the rate at which a wave changes in space to the rate at which it changes in time.

$$\nabla^2\Psi = \frac{1}{v^2}\frac{\partial^2\Psi}{\partial t^2} \tag{3.3}$$

where ∇^2 (called the Laplacian) represents how the wave spreads in space, and v is the velocity of the wave. It tells us that any disturbance in a medium will spread out as a wave. In electromagnetism, Maxwell showed that both electric and magnetic fields satisfy this same equation. This means that light itself behaves like a wave — specifically, an electromagnetic wave that can travel even through a vacuum.

3.1.3 Maxwell's Equations

Maxwell's equations form the foundation of electromagnetism, describing the relationship and interaction between electric and magnetic fields. These four fundamental laws unify electricity, magnetism, and light into a single comprehensive framework. They illustrate how electric charges generate electric fields, how currents and time-varying electric fields give rise to magnetic fields, and how both fields propagate together as electromagnetic waves. In this section, each equation is explained in simple terms to provide a clear understanding of its concept and significance.

Gauss's Law for Electricity

The first of Maxwell's equations, known as Gauss's Law for Electricity, explains how electric charges are linked to the electric field they generate. The mathematical expression of this law is given as

$$\nabla \cdot \mathbf{E} = \frac{\rho}{\varepsilon_0} \tag{3.4}$$

where $\mathbf{E}$, ρ is the electric charge density, and ε_0 is the permittivity of free space.

This equation explains that electric charges are the origin of electric fields. A positive charge generates an electric field that extends outward, while a negative charge creates one that points inward. In simple terms, the law states that the total electric flux passing through a closed surface depends on the amount of charge contained within that surface. If there is no charge inside, the number of field lines entering and leaving the surface are equal, so the net flux is zero.

Gauss's Law is especially useful for calculating electric fields when the charge distribution exhibits significant symmetry, such as spherical, cylindrical, or planar forms. For example, it enables the determination of the electric field around a charged sphere or a long charged wire without the need for complex calculus. This law helps us understand how electric fields behave around conductors, insulators, and in capacitors, where charges accumulate on surfaces.

Gauss's Law for Magnetism

The second of Maxwell's equations is called Gauss's Law for Magnetism. It describes the nature of magnetic fields and is written as

$$\nabla \cdot \mathbf{B} = 0 \tag{3.5}$$

where $\mathbf{B}$ is the magnetic field. This equation states that the divergence of the magnetic field is zero, meaning that the magnetic field always forms closed loops.

Gauss's Law for Magnetism means that magnetic monopoles don't exist. You can't have just a north or just a south pole by itself. Every magnet always has both a north and a south pole. If you cut a magnet in half, each piece will still have both poles. This is different from electric charges, where positive and negative charges can exist separately.

Faraday's Law of Induction

The third of Maxwell's equations is called Faraday's Law of Electromagnetic Induction. It shows that a changing magnetic field can create an electric field. The equation is written as

$$\nabla \times \mathbf{E} = -\frac{\partial \mathbf{B}}{\partial t} \tag{3.6}$$

where $\nabla \times \mathbf{E}$ represents the curl of the electric field and $\frac{\partial \mathbf{B}}{\partial t}$ is the rate of change of the magnetic field with time. The negative sign shows that the direction of the induced electric field opposes the change in magnetic flux, according to Lenz's Law.

In simple terms, Faraday's Law means that when the magnetic field in a region of space changes, it produces an electric field. This changing magnetic field can come from a moving magnet, a changing current, or any process that alters the magnetic flux. The produced electric field can drive a current in a closed loop of wire, which is the basic principle of electric generators, transformers, and induction motors.

Faraday's Law is one of the most important discoveries in physics and engineering. It is the reason we can generate electricity on a large scale. This changing flux induces an electric current, which we use as electric power. It also plays an important role in wireless charging and in the operation of sensors and antennas.

Ampère–Maxwell Law

The fourth and final equation is called the Ampère–Maxwell Law. It describes how magnetic fields are generated both by electric currents and by changing electric fields. The equation can be written as

$$\nabla \times \mathbf{B} = \mu_0 \mathbf{J} + \mu_0 \varepsilon_0 \frac{\partial \mathbf{E}}{\partial t} \tag{3.7}$$

where $\nabla \times \mathbf{B}$ is the curl of the magnetic field, $\mathbf{J}$ is the current density, μ_0 is the permeability of free space, and ε_0 is the permittivity of free space. The first term on the right-hand side represents the magnetic field created by an electric current, while the second term (added by Maxwell) represents the magnetic field created by a changing electric field.

This law extends Ampère's original law by adding the displacement current term $\mu_0 \varepsilon_0 \frac{\partial \mathbf{E}}{\partial t}$. This addition was crucial because it made the set of equations consistent even when there was no physical current present, such as in a capacitor, where the electric field changes over time. Maxwell realized that a time-varying electric field could act like a current and produce a magnetic field, just like a real current does.

The Ampère–Maxwell Law beautifully shows the symmetry between electricity and magnetism. A changing electric field produces a magnetic field, and as Faraday's Law shows, a changing magnetic field produces an electric field. This continuous interaction allows electromagnetic waves to travel through space. When these two fields support each other, they form a self-propagating wave — this is what light actually is. The speed of these waves in free space is given by

$$c = \frac{1}{\sqrt{\mu_0 \varepsilon_0}} \tag{3.8}$$

which is the speed of light. This connection proved that light is an electromagnetic phenomenon and unified the fields of electricity, magnetism, and optics into one complete theory.

Maxwell's equations not only describe how electromagnetic waves travel but also form the foundation of many technologies we use today — from radio and communication systems to medical imaging and optical sensors.

3.2 Interaction of Light with Matter

The interaction of light with material causes several physical processes to occur, such as reflection, transmission, absorption, and scattering. The way light behaves depends strongly on the material's optical properties, which are determined by its electronic structure and how the electrons respond to the oscillating electric field of the light wave. To understand these interactions, materials are generally classified into three main categories: dielectrics, metals, and semiconductors.

3.2.1 Dielectric Materials

Dielectrics are insulating materials that do not have free charge carriers. When an electromagnetic wave passes through a dielectric, the bound electrons inside the atoms are displaced slightly from their equilibrium positions, producing an induced electric dipole moment. These dipoles oscillate with the applied electric field, giving rise to polarization. The strength of this polarization depends on the permittivity of the material.

In dielectrics, the electric field is not completely blocked but rather slowed down. The phase velocity of light inside a dielectric is given by

$$v = \frac{c}{n} \tag{3.9}$$

where c is the speed of light in vacuum and n is the refractive index of the material. Common dielectric materials include glass, silicon dioxide (SiO_2), and various oxides such as tantalum pentoxide (Ta_2O_5). These materials are widely used in optics and photonics because of their transparency and low absorption in the visible and near-infrared ranges.

3.2.2 Metallic Materials

In metals, a large number of free electrons are available for conduction. When an electromagnetic wave strikes a metal surface, the free electrons move easily in response to the oscillating electric field. This movement produces strong reflection and significant absorption of light. Because of this, metals are generally opaque to visible light and highly reflective.

The optical properties of metals can be described by their complex permittivity, which is given by

$$\varepsilon = \varepsilon' + j\varepsilon'' \tag{3.10}$$

where ε' represents the real part (related to how much the material stores electric energy) and ε'' represents the imaginary part (related to energy loss due to absorption). The negative value of ε' in metals at optical frequencies is responsible for unique phenomena such as surface plasmons, where electrons oscillate collectively along the surface of the metal.

3.2.3 Semiconductor Materials

Semiconductors have electrical properties between those of conductors and insulators. Their behavior depends on temperature, doping concentration, and wavelength of light. When photons with enough energy are absorbed, electrons in the valence band can jump to the conduction band, leaving behind holes. This process allows semiconductors to interact strongly with light, making them essential for devices like photodetectors, LEDs, and solar cells.

The optical constants of semiconductors vary with wavelength, and their refractive index can be tuned by altering their composition or by applying external electric fields. Materials such as silicon (Si) and gallium arsenide (GaAs) are commonly used in integrated photonics and plasmonic hybrid structures.

3.2.4 Complex Permittivity and Refractive Index

Light material interaction is determined by its complex permittivity ε and permeability μ. The complex refractive index is given by

$$\tilde{n} = n + ik \tag{3.11}$$

where n is the real part, representing the phase velocity of light, and k is the extinction coefficient, which indicates how strongly the material absorbs the light. The relation of the complex refractive index and the complex permittivity is

$$\tilde{n}^2 = \varepsilon_r = \varepsilon' + i\,\varepsilon'' \tag{3.12}$$

When ε'' is large, the material absorbs more light, leading to strong attenuation. On the other hand, a small ε'' value corresponds to transparent materials with minimal energy loss.

3.2.5 Reflection, Absorption, and Transmission

When light is incident at the boundary between two materials, part of the light is reflected, part is transmitted, and part may be absorbed. The reflection and transmission at normal incidence can be described using Fresnel's equations:

$$R = \left(\frac{n_1 - n_2}{n_1 + n_2}\right)^2, \qquad T = 1 - R - A \tag{3.13}$$

where R is reflectance, T is transmittance, and A is absorptance. For dielectrics, absorption is negligible, so $A \approx 0$ and $R + T = 1$. For metals, the imaginary part of the refractive index (k) causes strong absorption, reducing transmission drastically.

3.2.6 Dispersion of Light

Dispersion means that a material's refractive index varies according to the wavelength of light. It occurs because the oscillating electrons respond differently to different frequencies of the electromagnetic wave. In transparent materials, dispersion causes phenomena such as the separation of white light into colors through a prism. Mathematically, the variation of refractive index with wavelength can be expressed as

$$n(\lambda) = A + \frac{B}{\lambda^2} + \frac{C}{\lambda^4} \tag{3.14}$$

here A, B, and C are material-specific constants.

Dispersion is important in plasmonics because it affects the resonance conditions and propagation characteristics. Understanding the dispersion of both the dielectric and the metallic materials is essential when designing plasmonic waveguides and sensors.

3.2.7 Drude Model for Metals

The Drude model provides a theoretical explanation of how free electrons in metals respond to an applied electric field. Conduction electrons are regarded as a gas of charged particles that move freely but occasionally collide with ions in the lattice. According to the Drude model, the complex permittivity of a metal is given by

$$\varepsilon(\omega) = \varepsilon_\infty - \frac{\omega_p^2}{\omega^2 + i\gamma\omega} \tag{3.15}$$

where ε_∞ is the high-frequency permittivity, ω_p is the plasma frequency, and γ is the damping constant related to electron collisions.

Below the plasma frequency, the real part of ε becomes negative, causing the metal to reflect light strongly. At higher frequencies (above ω_p), the metal behaves more like a dielectric and becomes partially transparent. The Drude model successfully explains why metals like silver (Ag) and gold (Au) support surface plasmon resonances in the visible and near-infrared regions.

3.2.8 Lorentz Model for Dielectrics

While the Drude model explains the behavior of free electrons in metals, it does not accurately describe how bound electrons in dielectric or insulating materials respond to electromagnetic waves. To address this, the **Lorentz model** is used. This model assumes that electrons are bound to atoms or ions by a restoring force, similar to a spring, and that they can oscillate when an external electric field is applied.

In the Lorentz model, each bound electron is treated as a harmonic oscillator that experiences three main forces: the restoring force due to its bond with the nucleus, a damping force due to energy loss, and the driving force of the external electric field. The equation of motion for an electron under these forces can be written as

$$m\frac{d^2x}{dt^2} + m\gamma\frac{dx}{dt} + m\omega_0^2 x = -eE_0 e^{-i\omega t} \tag{3.16}$$

where m, γ, ω_0, e, $E_0 e^{-j\omega t}$ refer to the electron mass, damping coefficient, resonance frequency of the bound electron, electron charge, and the oscillating electric field, respectively.

By solving this equation, the induced polarization P in the material can be related to the electric field E through the electric susceptibility χ_e as

$$P = \varepsilon_0 \chi_e E \tag{3.17}$$

and the dielectric function (or permittivity) is given by

$$\varepsilon(\omega) = 1 + \chi_e(\omega) = 1 + \frac{Ne^2}{\varepsilon_0 m} \frac{1}{\omega_0^2 - \omega^2 - i\gamma\omega} \tag{3.18}$$

where N is the number of oscillating electrons per unit volume.

Near the resonance frequency ω_0, the material exhibits strong absorption and rapid changes in refractive index. The real part of $\varepsilon(\omega)$ determines how much the wave is slowed down, while the imaginary part represents energy loss due to absorption.

At frequencies much lower than the resonance frequency, the electrons follow the field almost instantaneously, and the material behaves like a regular dielectric with a constant positive permittivity. At frequencies close to ω_0, strong dispersion and absorption occur. Beyond the resonance frequency, the electrons cannot respond quickly enough, leading to a decrease in ε'. This frequency-dependent behavior explains why many dielectric materials have different refractive indices at different wavelengths.

3.2.9 Comparison Between Drude and Lorentz Models

The Drude and Lorentz models are often combined to elaborate on the optical response of real materials. The Drude model applies to *free electrons* (as in metals), while the Lorentz model applies to *bound electrons* (as in dielectrics or semiconductors). In fact, many materials can be modeled using a sum of several Lorentz oscillators to represent multiple electronic resonances. The combined form of the dielectric function can be expressed as

$$\varepsilon(\omega) = \varepsilon_\infty - \frac{\omega_p^2}{\omega^2 + i\gamma_D\omega} + \sum_j \frac{f_j\, \omega_{p,j}^2}{\omega_{0,j}^2 - \omega^2 - i\gamma_j\omega} \tag{3.19}$$

where the first term represents the background (high-frequency) permittivity, the second term is the Drude (free-electron) contribution, and the summation represents multiple Lorentz oscillators for bound-electron resonances with oscillator strengths f_j.

This combined model provides a realistic description of how metals, semiconductors, and dielectric materials interact with light over a wide frequency range. It helps explain optical phenomena such as color dispersion in glasses, plasma reflection in metals, and resonance absorption in semiconductors. In the context of plasmonics, understanding both models is essential for accurately predicting surface plasmon resonances and optimizing material choices for sensing or waveguiding applications.

3.3 Surface Plasmon

Surface plasmon theory explains the interaction between light and the collective oscillations of free electrons at the interface of a metal and a dielectric. These oscillations produce electromagnetic surface waves known as surface plasmons. When these waves couple with an external electromagnetic field, they are termed surface plasmon polaritons (SPPs). This concept is fundamental to modern plasmonics and is essential for applications such as subwavelength light confinement, sensing, and photonic integration.

3.3.1 Concept of Surface Plasmons

In a metal, free electrons can oscillate collectively relative to the fixed positive ion background. When these oscillations occur, the resulting electromagnetic wave is attached to the surface. This wave decays exponentially in both directions — into the metal and into the dielectric — creating a bound surface mode.

The surface plasmon can be visualized as a coupled excitation of photons and electron oscillations. Because the electric field of an SPP decays away from it, the energy is tightly confined to a smaller region. This confinement enables light manipulation at the nanoscale, far beyond the diffraction limit of conventional optics.

3.3.2 Derivation of the Dispersion Relation

At the interface, the electromagnetic fields must satisfy Maxwell's equations as well as the boundary conditions.

For a transverse-magnetic (TM) polarized wave, in which the magnetic field is parallel to the interface and the electric field has both normal and tangential components, the fields in each medium can be described as follows

$$E_{x,i}(z) = E_{0,i}\, e^{-\kappa_i|z|}\, e^{i(\beta x-\omega t)}, \qquad H_{y,i}(z) = H_{0,i}\, e^{-\kappa_i|z|}\, e^{i(\beta x-\omega t)} \tag{3.20}$$

where β is the propagation constant along the interface, ω is the angular frequency, and κ_i represents the decay constant in each medium ($i = m, d$).

From Maxwell's equations, the following relations hold for each medium:

$$\kappa_i^2 = \beta^2 - k_0^2\varepsilon_i, \qquad k_0 = \frac{\omega}{c} \tag{3.21}$$

where $k_0 = \omega/c$ is the free-space wavenumber. According to the boundary conditions, the tangential components of E and H must be continuous across the interface. Upon applying the boundary condition, the dispersion relation for the surface plasmon polariton is yielded.

$$\frac{\kappa_d}{\varepsilon_d} + \frac{\kappa_m}{\varepsilon_m} = 0 \tag{3.22}$$

By substituting for κ_i, we obtain the general expression for the propagation constant β:

$$\beta = k_0\sqrt{\frac{\varepsilon_m\varepsilon_d}{\varepsilon_m+\varepsilon_d}} \tag{3.23}$$

3.3.3 Properties of Surface Plasmon Polaritons

The propagation constant β is complex because ε_m is complex. The real part tells us how fast the plasmon wave travels, while the imaginary part indicates how much the wave loses energy due to absorption in the metal. The effective wavelength of the surface plasmon polariton (SPP) is shorter than the wavelength of light in the surrounding material, which means the wave is very tightly confined to the surface where the metal and dielectric meet..

The condition for an SPP to exist requires the real part of ε_m to be negative and its magnitude larger than that of ε_d, i.e.,

$$\text{Re}(\varepsilon_m) < -\varepsilon_d \tag{3.24}$$

This condition is typically satisfied by noble metals such as gold (Au) and silver (Ag) in the visible and near-infrared spectral regions. The field penetration depth into the dielectric and metal is given by

$$\delta_d = \frac{1}{\kappa_d}, \qquad \delta_m = \frac{1}{\kappa_m} \tag{3.25}$$

showing that most of the energy resides in the dielectric side, which makes the SPP extremely sensitive to any change in the refractive index of the surrounding medium.

3.3.4 Excitation of Surface Plasmons

Direct excitation of surface plasmons by light incident from air or a dielectric is not possible because of the momentum mismatch between the photon and the SPP. Various coupling methods are used to overcome this mismatch, such as:

- **Prism coupling** (Kretschmann or Otto configuration): A thin metal film is attached to a high-index prism, allowing the incident light to achieve the necessary in-plane momentum.
- **Grating coupling**: A periodic metallic structure provides additional momentum components to match the plasmon wavevector.
- **Waveguide coupling**: Optical waveguide modes can be engineered to interact with SPPs at the interface.

The coupling condition is achieved when the parallel component of the incident light wavevector matches the SPP propagation constant:

$$k_x = \beta_{\text{SPP}} \tag{3.26}$$

At this resonance condition, a sharp dip in reflected light intensity can be observed — this is known as the **plasmon resonance**.

3.3.5 Plasmon Resonance and Energy Localization

Plasmon resonance happens when the light's frequency matches the natural vibration frequency of the electrons on the surface. At this point, the surface charges vibrate a lot, making the local electric field near the surface much stronger. This resonance is very sensitive to changes around it. Even a tiny change in the refractive index of the material next to the metal can change the resonance, and this is the main idea used in many plasmonic sensors. The resonance wavelength λ_{res} can be tuned by changing the metal type, the dielectric material, or the geometry of the interface.

3.3.6 Localized Surface Plasmon Resonance (LSPR)

When a metal nanoparticle is much smaller than the wavelength of the light hitting it, the free electrons inside the particle can move together in response to the light's electric field. This effect is called localized surface plasmon resonance.

In LSPR, confinement of the electric field occurs around the nanoparticle rather than along an extended surface. The resonance frequency depends on the size, shape, and dielectric environment of the nanoparticle. The condition for resonance can be approximated using the quasi-static approximation, which gives

$$\text{Re}[\varepsilon_m(\omega_{\text{res}})] = -2\,\varepsilon_d \tag{3.27}$$

for a spherical nanoparticle. At this frequency, the local field enhancement near the particle surface can be several orders of magnitude larger than the incident field.

LSPR is the foundation for many sensing and spectroscopy techniques like surface-enhanced Raman scattering (SERS) and color-based biosensing. Because the localized fields react strongly to changes in the surrounding refractive index, LSPR sensors can detect molecular interactions even at very low concentrations.

In simple terms, surface plasmons are groups of electrons that oscillate together at the interface between a metal and a dielectric material. When these electron waves couple with light waves, they form surface plasmon polaritons (SPPs), which let light be confined and directed on a scale smaller than the usual diffraction limit. The way these SPPs travel is described by a relation from Maxwell's equations.

Localized surface plasmons, which occur in tiny nanoparticles, create a strong enhancement of the electric field and are very sensitive to their environment. This makes them especially useful in sensing, imaging, and various nanophotonics applications.

3.4 Metal–Insulator–Metal (MIM) Waveguide

MIM waveguide is a fundamental structure in plasmonics that allows light to be confined and guided at dimensions much smaller than the free-space wavelength. It is composed of a thin dielectric (insulating) layer sandwiched between two metallic layers. The strong field confinement in the dielectric region arises from the coupling of SPPs at the two metal–dielectric interfaces. Because of their deep subwavelength confinement, MIM waveguides are widely used in plasmonic circuits, sensors, and nanophotonic devices.

3.4.1 Structure and Working Principle

The basic structure of an MIM waveguide is shown schematically as two semi-infinite metallic regions separated by a thin dielectric core of thickness d. The wave propagates along the x-direction, and the z-axis is perpendicular to the interfaces. The dielectric core has a permittivity ε_d, while the metal claddings have complex permittivity ε_m.

In this configuration, SPPs can exist at each metal–dielectric interface. When the dielectric layer is sufficiently thin, the SPP modes at both interfaces overlap and couple with each other, forming symmetric and antisymmetric hybrid modes. The resulting field confinement inside the dielectric layer depends on the thickness d and the optical properties of the materials.

The MIM waveguide supports only TM modes, where the magnetic field is perpendicular to the plane of incidence (along the y-axis), and the electric field has both x and z components.

3.4.2 Field Distribution in the MIM Waveguide

For TM-polarized waves propagating in the x-direction, the magnetic field component in each region can be written as

$$E_z(z) = \begin{cases} Ae^{\kappa_m(z+d/2)}, & z < -d/2 \text{ (Lower metal);} \\ B\cosh(\kappa_d z) + C\sinh(\kappa_d z), & |z| \leq d/2 \text{ (Dielectric);} \\ De^{-\kappa_m(z-d/2)}, & z > d/2 \text{ (Upper metal).} \end{cases} \tag{3.28}$$

where κ_m and κ_d are the decay constants in the metal and dielectric, respectively. These are related to the propagation constant β by

$$\kappa_m^2 = \beta^2 - k_0^2\varepsilon_m, \qquad \kappa_d^2 = \beta^2 - k_0^2\varepsilon_d \tag{3.29}$$

where $k_0 = \omega/c$ is the free-space wavenumber.

The fields decay exponentially in the metal regions, indicating that the energy is confined primarily within the dielectric layer. The boundary condition of the electric and magnetic fields at the interfaces provides the conditions needed to determine β.

3.4.3 Mode Analysis

Applying the boundary conditions at $z = \pm d/2$ leads to the characteristic dispersion relations for the supported modes. Two types of modes can exist depending on the symmetry of the field distribution:

Symmetric Mode:

$$\tanh\left(\frac{\kappa_d d}{2}\right) = -\frac{\varepsilon_m \kappa_d}{\varepsilon_d \kappa_m} \tag{3.30}$$

Antisymmetric Mode:

$$\coth\left(\frac{\kappa_d d}{2}\right) = -\frac{\varepsilon_m \kappa_d}{\varepsilon_d \kappa_m} \tag{3.31}$$

The symmetric mode has an even magnetic field distribution in the dielectric region, while the antisymmetric mode has an odd distribution. The propagation constants of these modes differ, with the antisymmetric mode generally exhibiting stronger confinement but higher loss.

3.4.4 Effective Index and Propagation Length

The effective refractive index of the mode is defined as

$$n_{\text{eff}} = \frac{\beta}{k_0} \tag{3.32}$$

This parameter indicates how much slower the guided mode travels compared to light in free space. A larger n_{eff} implies stronger field confinement but also typically higher propagation losses.

The propagation length, which quantifies how far the mode can travel before its intensity decays to $1/e$ of its initial value, is given by

$$L_p = \frac{1}{2\,\text{Im}(\beta)} \tag{3.33}$$

A trade-off exists between confinement and propagation length: stronger confinement increases losses due to the higher overlap of the field with the lossy metal regions.

3.4.5 Mode Confinement

The field confinement can be quantified by examining how deeply the field penetrates into the metal and dielectric regions. The decay lengths in each region are given by

$$\delta_d = \frac{1}{\kappa_d}, \qquad \delta_m = \frac{1}{\kappa_m} \tag{3.34}$$

For metals such as gold or silver, δ_m is typically a few tens of nanometers in the visible range, while δ_d may range from tens to hundreds of nanometers depending on the dielectric material. As the dielectric layer thickness decreases, the fields from the two interfaces interact more strongly, increasing the confinement but also enhancing ohmic losses.

3.4.6 Advantages and Applications of MIM Waveguides

MIM waveguides provide several advantages over single-interface plasmonic structures:

- They offer extreme subwavelength confinement, enabling the design of ultra-compact photonic components.
- They are compatible with planar fabrication processes, making them suitable for integrated plasmonic circuits.
- They support flexible mode engineering by adjusting the dielectric thickness and material properties.

Because of these advantages, MIM waveguides are used in various applications such as:

- **Plasmonic waveguides and couplers:** guiding and routing optical signals at nanoscale dimensions.
- **Plasmonic sensors:** exploiting field confinement to enhance sensitivity to refractive index changes.
- **Nanoantennas and filters:** enabling wavelength-selective light localization.

In conclusion, we can say that, the metal–insulator–metal waveguide supports tightly confined plasmonic modes that propagate along the dielectric core sandwiched between two metal layers. The coupling of SPPs at both interfaces results in symmetric and antisymmetric modes governed by specific dispersion relations. While MIM waveguides provide exceptional field confinement, they suffer from high propagation losses due to the absorption in metals. Nonetheless, their ability to manipulate light at nanoscale dimensions makes them key components in plasmonic and nanophotonic device design.

3.5 Refractive Index Sensing Principle

One of the most important applications of plasmonic structures is in refractive index sensing. The main principle is that the optical properties of SPRs depend strongly on the dielectric environment near the metal surface. When the refractive index of the surrounding medium changes, it alters the resonance condition of the surface plasmon, resulting in a measurable shift in wavelength, angle, or intensity. This susceptibility to small refractive index variations enables the detection of chemical, biological, and environmental changes at extremely low concentrations.

3.5.1 Fundamental Working Principle

When light hits the surface where a metal meets a non-metal material, it makes the free electrons in the metal move together in waves called surface plasmons. How these waves form depends on the properties of both the metal(ε_m) and the material(ε_d) around it. The way these surface waves, called SPPs, travel along the interface can be described by the following formula that includes the characteristics of both the metal and its surrounding material.

$$\beta_{\text{SPP}} = k_0 \sqrt{\frac{\varepsilon_m \varepsilon_d}{\varepsilon_m + \varepsilon_d}} \tag{3.35}$$

where $k_0 = 2\pi/\lambda$ is the free-space wavenumber. Any change in ε_d, which corresponds to a change in the refractive index $n_d = \sqrt{\varepsilon_d}$ of the surrounding medium, modifies β_{SPP}. As a result, the resonance wavelength λ_{res} shifts.

This shift forms the basis of refractive index sensing. By monitoring the change in resonance wavelength or angle, one can determine the amount of refractive index change, which is often caused by the adsorption of molecules or variations in the ambient medium.

3.5.2 Sensitivity

The sensitivity (S) of a plasmonic sensor indicates the extent to which the resonance wavelength shifts in response to variations in the refractive index of the surrounding environment. It is mathematically defined as

$$S_\lambda = \frac{\Delta\lambda_{\text{res}}}{\Delta n} \tag{3.36}$$

where $\Delta\lambda_{\text{res}}$ and Δn denote the shift in resonance wavelength and change in refractive index respectively. The unit of sensitivity is usually in nm/RIU.

A higher sensitivity means that the plasmonic mode responds strongly to small changes in the environment. Sensitivity depends on factors such as the choice of metal, the thickness of the dielectric layer, the mode confinement, and the structure geometry. For instance, MIM waveguides and nanoparticle-based sensors often show high sensitivity due to their strong electromagnetic field confinement at the metal–dielectric interface.

3.5.3 Figure of Merit (FOM)

While sensitivity indicates how much the resonance wavelength shifts, it does not account for the sharpness of the resonance curve. Therefore, another important parameter, the FOM, is introduced to measure the sensing performance more accurately. It is defined as

$$\text{FOM} = \frac{S_\lambda}{\text{FWHM}} \tag{3.37}$$

A higher FOM indicates not only high sensitivity but also a narrow resonance peak, which makes it easier to detect small changes in the refractive index. Optimizing FOM involves achieving strong field confinement (for higher sensitivity) while minimizing losses and damping (to reduce FWHM). Materials such as silver (Ag) and gold (Au) are often preferred due to their low optical losses and stable plasmonic response in the visible and near-infrared regions.

3.5.4 Resolution

The resolution of a plasmonic sensor defines the smallest detectable change in refractive index that can be measured reliably. It is inversely related to sensitivity and depends on the precision of the detection system. The resolution can be expressed as

$$R = \frac{\Delta n_{\text{min}}}{\text{Signal-to-Noise Ratio (SNR)}} \tag{3.38}$$

In practice, the resolution is determined by how small a wavelength or intensity shift can be measured relative to the noise level of the optical detection system. High-resolution sensors are essential for detecting trace amounts of biomolecules or chemicals.

3.5.5 Types of Plasmonic Sensing Mechanisms

Plasmonic sensing can be achieved in various configurations, depending on how the resonance condition is monitored. The main categories include wavelength-shift, angular-shift, and intensity-based detection methods.

- **Wavelength-Shift Based Sensing:** In this method, the resonance wavelength changes as the refractive index of the sensing medium changes. The sensor measures the spectral shift in reflection or transmission intensity. This approach is widely used in both SPR and LSPR sensors.

- **Angular-Shift Based Sensing:** The resonance condition can also be detected by monitoring the angle at which light couples into surface plasmons. A change in refractive index shifts the resonance angle, which can be measured using a prism-based Kretschmann configuration. This approach is commonly used in commercial SPR systems.

- **Intensity-Based Sensing:** Instead of measuring shifts in wavelength or angle, some sensors operate at a fixed wavelength and monitor changes in reflected or transmitted intensity. This technique is simpler and faster but generally less precise.

Each method has its advantages. Wavelength-based sensing provides high accuracy, angular-based methods are well-suited for bulk sensing, and intensity-based detection is ideal for low-cost and portable systems.

3.5.6 Performance Optimization

The performance of plasmonic refractive index sensors can be improved by optimizing several parameters:

- **Material Selection:** Choosing metals with low damping (such as Ag or Au) minimizes loss and enhances resonance sharpness.

- **Dielectric Engineering:** Using high-index dielectric layers can improve confinement and enhance interaction with the analyte.

- **Geometric Design:** Adjusting the waveguide width, film thickness, or nanoparticle geometry can tune the resonance wavelength and sensitivity.

- **Hybrid Structures:** Combining plasmonic and dielectric waveguides (e.g., MIM with dielectric ridge) can balance confinement and propagation loss.

3.6 Simulation or Analytical Modeling Approach

In addition to theoretical analysis, numerical simulation plays a vital role in understanding and designing plasmonic and photonic structures. Because the electromagnetic behavior of plasmonic devices often involves complex geometries and materials with frequency-dependent permittivity, analytical solutions are rarely possible. Therefore, computational modeling methods such as the FEM, FDTD, and Transfer Matrix Method (TMM) are commonly employed to solve Maxwell's equations under realistic boundary conditions. Among these, FEM is one of the most flexible and accurate approaches for simulating plasmonic waveguides and sensors.

3.6.1 Finite Element Method (FEM)

It is a numerical approach used to obtain approximate solutions for partial differential equations, such as Maxwell's equations, by dividing the simulation domain into small, finite elements. Within each element, the field quantities are expressed using interpolation (basis) functions. FEM transforms the continuous problem into a discrete matrix equation that can be solved efficiently using computational software such as COMSOL Multiphysics, ANSYS HFSS, or CST Studio Suite.

In the context of electromagnetic wave propagation, the governing equation derived from Maxwell's curl–curl formulation is expressed as

$$\nabla \times \left(\mu_r^{-1} \nabla \times \mathbf{E}\right) - k_0^2 \varepsilon_r \mathbf{E} = 0 \tag{3.39}$$

where $\mathbf{E}$ is the electric field vector, μ_r and ε_r are the relative permeability and permittivity of the material, respectively, and $k_0 = \omega/c$ is the free-space wavenumber.

To use FEM, the area is divided into many small shapes (usually triangles in 2D or tetrahedrons in 3D). The electric field inside each small shape is estimated using certain simple functions. A method called the Galerkin method is used to get an easier form of the equation. Special boundary layers called perfectly matched layers (PMLs) are added to absorb waves that leave the area, so they don't bounce back inside.

3.6.2 Boundary Conditions and Meshing

Accurate boundary conditions are essential for reliable simulation results. Commonly used conditions include:

- **Perfectly Matched Layer (PML):** an artificial absorbing layer that simulates open boundaries to ensure that waves leaving the structure do not reflect back into the computational domain.
- **Port Boundary Condition:** defines excitation and output boundaries where power is injected or measured.
- **Symmetry Boundaries:** reduce computational cost by exploiting the structural symmetry of the design.

Meshing plays a crucial role in determining accuracy and computational cost. Finer meshes are needed in regions with strong field gradients, such as near metal–dielectric interfaces, where the field varies rapidly due to plasmonic confinement. Adaptive meshing algorithms automatically refine the mesh until the solution converges within a specified tolerance.

3.6.3 Material Modeling and Dispersion

In plasmonic simulations, it is important to use realistic, frequency-dependent optical constants for metals and dielectrics. These properties are usually obtained from experimental data or analytical models such as the Drude or Drude–Lorentz model. The complex permittivity $\varepsilon(\omega)$ describes both the phase velocity and absorption of the electromagnetic wave in the material. For frequency-domain FEM simulations, $\varepsilon(\omega)$ is directly assigned as a complex parameter, while in time-domain simulations, the dispersion is implemented using auxiliary differential equations.

3.6.4 Calculation of Key Parameters

After solving for the field distributions, several key quantities can be derived to evaluate the performance of the plasmonic structure:

- **Effective Refractive Index:**
$$n_{\text{eff}} = \frac{\beta}{k_0} \tag{3.40}$$
where β is obtained from the phase variation of the mode along the propagation direction.

- **Propagation Length:**
$$L_p = \frac{1}{2\,\text{Im}(\beta)} \tag{3.41}$$
which indicates how far the mode travels before its intensity decays to $1/e$ of its initial value.

- **Field Confinement:** determined by examining the spatial decay of the field amplitude from the core into the cladding materials.

- **Power Flow:** calculated using the Poynting vector
$$\mathbf{S} = \frac{1}{2}\,\text{Re}\left(\mathbf{E} \times \mathbf{H}^*\right) \tag{3.42}$$
, which provides information about the energy transport within the structure.

Chapter 4

Properties of Materials

4.1 Silver (Ag), Gold (Au), and Silver-Gold (Ag-Au) alloy

Gold (Au) and silver (Ag) are transition metals belonging to Group 11 of the periodic table, often referred to as the coinage metals. Silver has an atomic number of 47 and lies in period 5, while gold has an atomic number of 79 and lies in period 6. Both exhibit high electrical and thermal conductivity, characteristic metallic luster, and strong plasmonic behavior due to their single valence s-electron outside a filled d subshell.

The drive to find new plasmonic materials is mainly due to the limitations of Ag and Au as the base materials of plasmonic sensors and the combination of individual advantages gained from the materials. Ag and Au are used because they show strong surface plasmon resonance (SPR) in the visible light wave range and beyond and also because of their high dielectric constant, which helps in both localized and propagating modes of surface plasmons [85][86]. Plasmonic sensors made of silver have higher sensitivity than gold sensors [13]. This is due to the low damping and the strong plasmonic coupling, which increases the quality of detection [14]. But the chemical stability of silver is very poor, and it goes through oxidation and other chemical reactions [13][14]. Gold plasmonic sensors do not face these problems [14]. But gold has wider resonant curves [15] which reduce the quality of detection. In order to combine the advantages, an alloy of gold and silver is used. These alloys provide better sensitivity than their monometallic counterparts. Hwang et al. showed that the Ag-Au-made plasmonic sensors show a 40% increase in sensitivity in the infrared region compared to their monometallic counterparts [87]. The alloy also shows a narrow bandwidth compared to that of gold and high stability in harsh chemical environments [88]. In some cases, the stability of the Ag-Au nanoparticle is more than pure gold nanoparticles due to the charge compensation mechanism in the alloy [89][90]. Another advantage of using Ag-Au nanoparticles is that they have tunable plasmon resonance. By varying the ratio of silver and gold, the resonant wavelength can be customized according to requirements. These alloys also exhibit greater absorption and scattering cross-sections [91]. There are a number of procedures used to synthesize these Ag-Au alloy nanoparticles. These procedures include annealing at very high temperatures [88], chemical reduction methods[92], the seed-mediated growth approach [93], etc.

4.2 Tantalum pentoxide (Ta_2O_5)

Tantalum pentoxide (Ta_2O_5) has gained attention as an excellent candidate for plasmonic sensing applications owing to its distinctive blend of optical and physical characteristics. It possesses a high refractive index and a large optical band gap [16], both of which are advantageous for enhancing plasmonic field confinement. The high refractive index enables stronger localization of the electromagnetic field near the metal–dielectric interface, effectively concentrating the electric field closer to the sensor surface. This consequently strengthens the coupling between the evanescent plasmonic field and the surrounding sensing medium, leading to enhanced sensor sensitivity and improved signal-to-noise ratio.

Furthermore, tantalum pentoxide exhibits excellent optical transparency across the visible and near-infrared spectral regions, along with a remarkably high refractive index in this range [17]. These attributes make it an attractive dielectric layer in plasmonic and photonic structures where efficient light confinement and transmission are simultaneously required. Its wide band gap (approximately 4.0–4.5 eV) minimizes optical absorption losses, thus improving the quality factor of the plasmonic resonance. Beyond its optical merits, Ta_2O_5 also demonstrates exceptional thermal stability and chemical inertness [17], allowing it to maintain performance even under elevated temperatures or in reactive environments—conditions under which traditional noble metals such as silver and gold tend to degrade.

An additional advantage of tantalum pentoxide is its intrinsic ability to provide refractive index tunability through variations in deposition parameters, film thickness, or stoichiometric control [18]. This tunability introduces an extra degree of freedom in sensor design, enabling precise optimization of resonance conditions for different operating wavelengths and analyte environments. In recent studies, Ta_2O_5 has been employed in hybrid plasmonic architectures, often in combination with noble metals like silver and gold, to enhance the sensing performance [16, 17]. Such composite systems leverage the strong plasmonic activity of metals and the high-index dielectric properties of tantalum pentoxide, resulting in sharper resonance features, reduced propagation losses, and improved figures of merit compared with conventional metal-only plasmonic sensors. These findings highlight the growing importance of Ta_2O_5 as a dielectric material capable of advancing the sensitivity, tunability, and robustness of next-generation plasmonic refractive index sensors.

Chapter 5

Proposed Structure and Optimization

5.1 Initial structure and structural parameters

We have proposed a plasmonic sensor having MIM configuration and it consists of an interdigitated resonator. A schematic of our proposed sensor is given below. Initially, we used silver (Ag) as the metal.

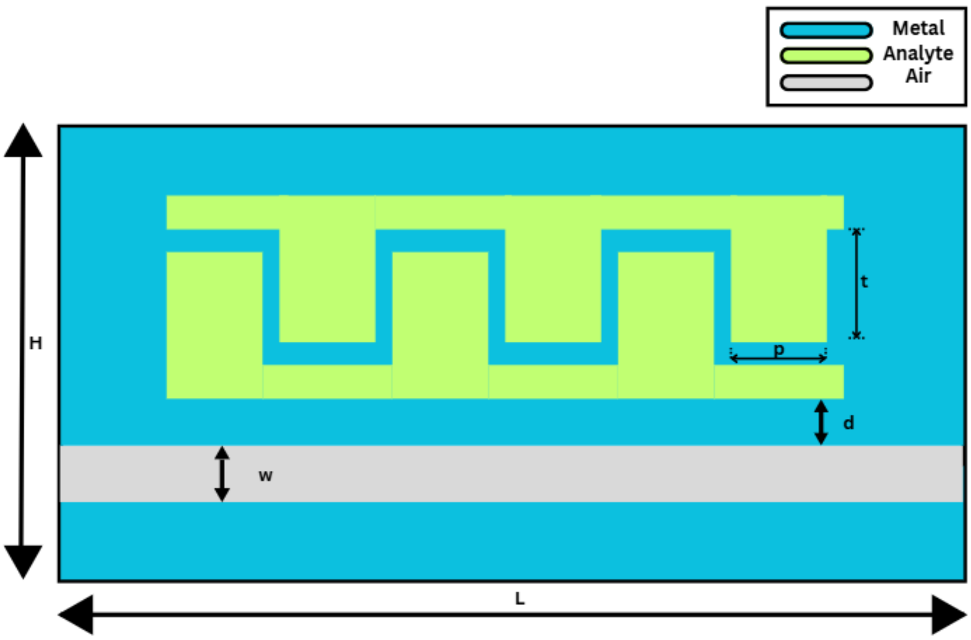

Figure 5.1: Proposed Structure

Structural Parameters:

- L = Length of the structure
- H = Height of the structure
- t = length of the interdigitated extensions
- p = width of the interdigitated extensions
- w = width of the waveguide
- d = distance between the resonator and the waveguide

Initial Dimentions:

- L = 800 nm
- H = 400 nm
- t = 70 nm
- p = 50 nm
- w = 50 nm
- d = 30 nm

Simulation Results:

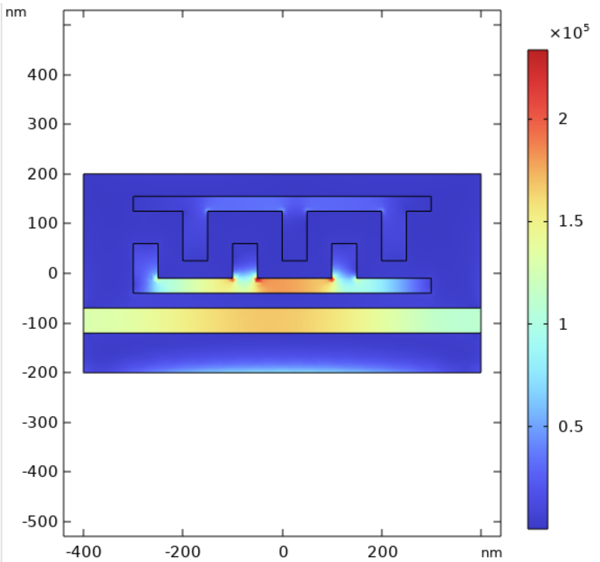

Figure 5.2: Electric field for initial structure

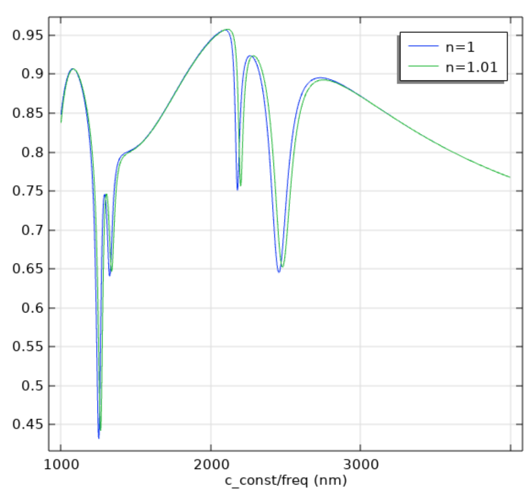

Figure 5.3: Simulation result for initial structure

Performance Parameters:

- Sensitivity = 2440 nm/RIU
- FWHM = 116.7 nm
- FOM = 20.9
- λ-resonant =2454 nm
- Q-factor = 21.03

5.2 Optimization of Structural Parameters

5.2.1 Optimization of length of the interdigitated extensions(t)

We vary 't' while keeping all other parameters constant at initial values. In such a case,

- L = 800 nm
- H = 400 nm
- p = 50 nm
- w = 50 nm
- d = 30 nm

We vary 't' from 70 nm to 100 nm with a step size of 10 nm and find the value for which we have the best output.

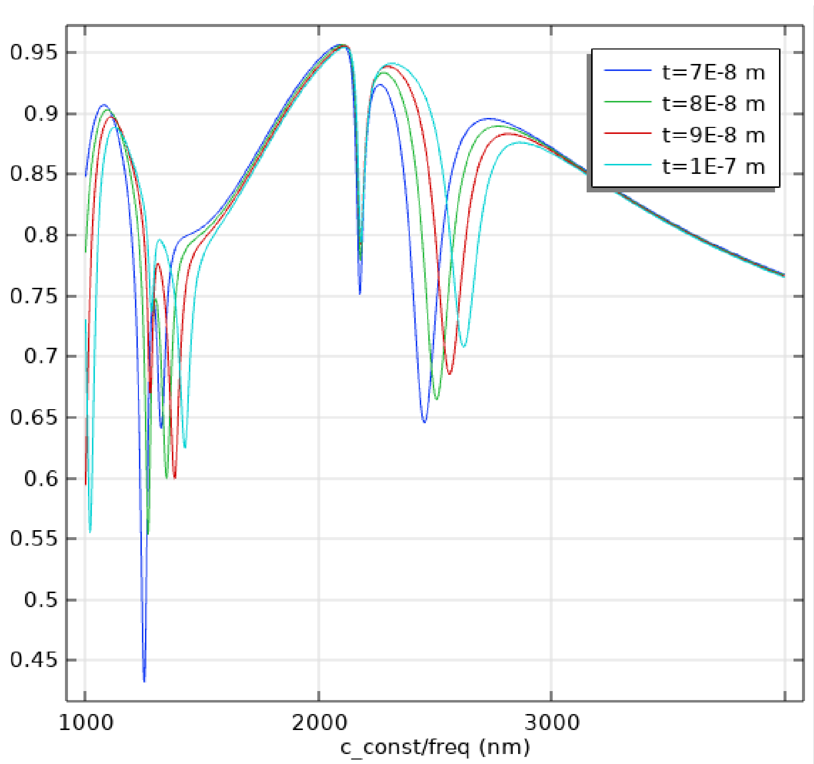

Figure 5.4: Variation of 't'

From the variation, we see that we obtain the best results for t = 100 nm, with a greater resonant wavelength and sensitivity. So now we fix t at 100 nm and find the performance parameters.

Simulation Results:

After fixing t = 100 nm, the following results are obtained.

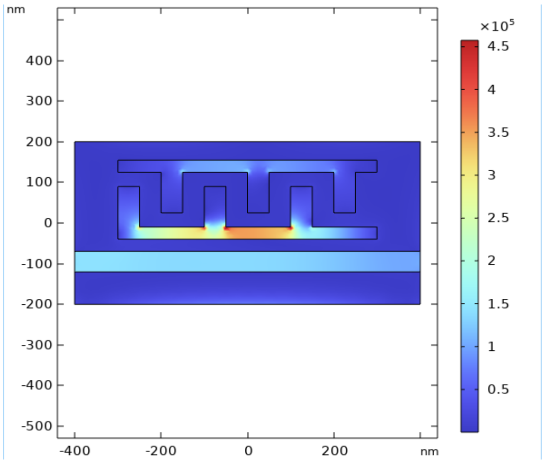

Figure 5.5: Electric field for optimized 't'

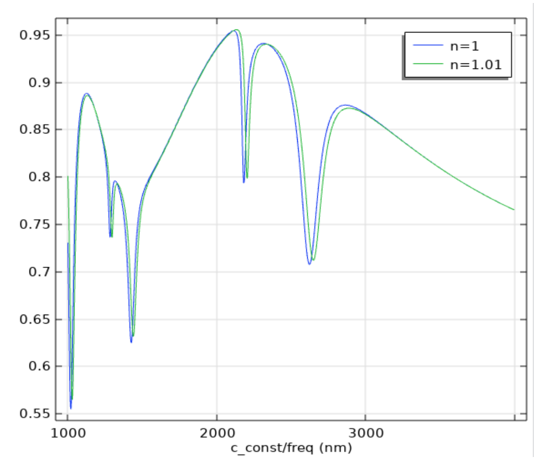

Figure 5.6: Simulation result for optimized 't'

Performance parameters:

- Sensitivity = 2600 nm/RIU
- FWHM = 116.5 nm
- FOM = 22.32
- λ-resonant =2623 nm
- Q-factor = 22.51

5.2.2 Optimization of width of the interdigitated extensions(p)

We vary 'p', keeping all other parameters constant at initial values. In this case,

- L = 800 nm
- H = 400 nm
- t = 100 nm
- w = 50 nm
- d = 30 nm

We vary 'p' from 50 nm to 85 nm with a step size of 5 nm and find the value for which we have the best output.

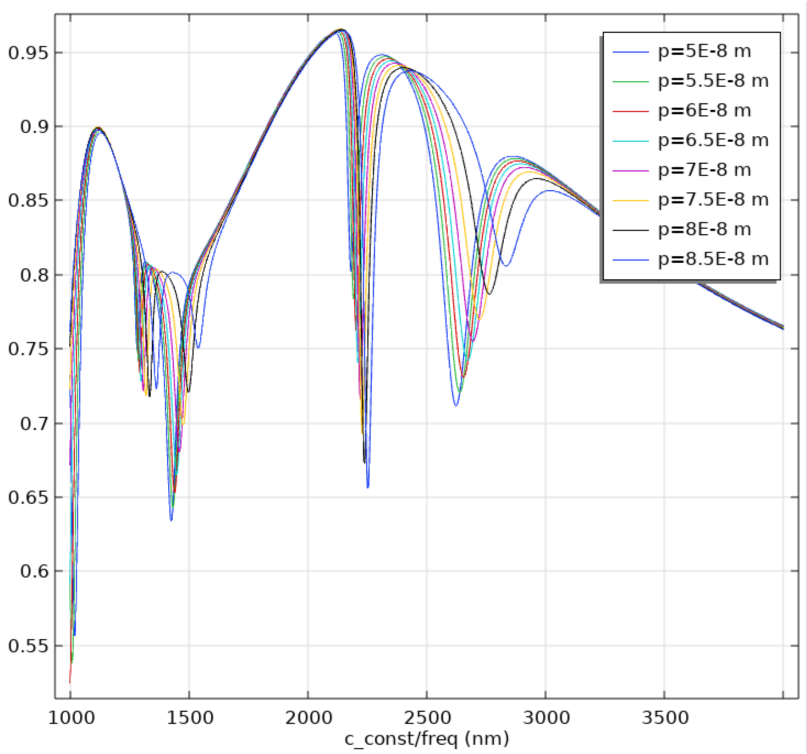

Figure 5.7: Variation of 'p'

From the variation, we see that we obtain the best results for p = 85 nm, with a greater resonant wavelength and sensitivity. So now we fix p at 85 nm and find the performance parameters.

Simulation results:

After setting p= 85 nm, the following results are obtained.

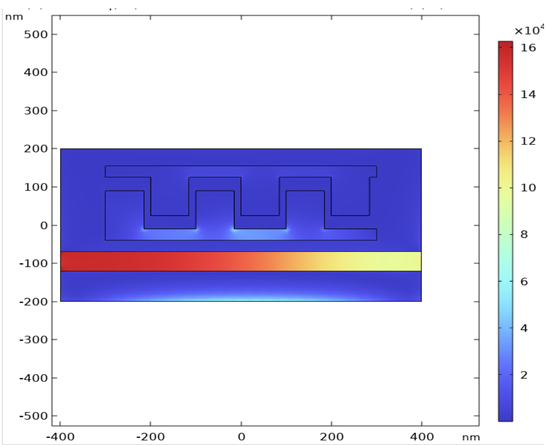

Figure 5.8: Electric field for optimized 'p'

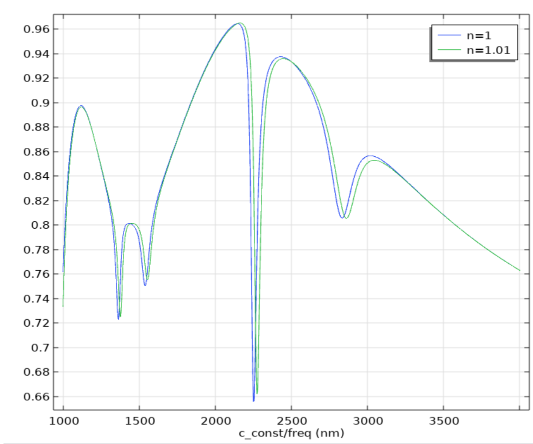

Figure 5.9: Simulation result for optimized 'p'

Performance parameters:

- Sensitivity = 2740 nm/RIU
- FWHM = 116.7 nm
- FOM = 23.47
- λ-resonant =2454 nm
- Q-factor = 21.03

5.2.3 Optimization of distance between resonator and waveguide (d)

We vary 'd', keeping all other parameters constant at initial values. In that case,

- L = 800 nm
- H = 400 nm
- t = 100 nm
- w = 50 nm
- p = 85 nm

We varied the distance d, from 10 nm to 50 nm, with a step size of 10 nm, and found the value for which we have the best output.

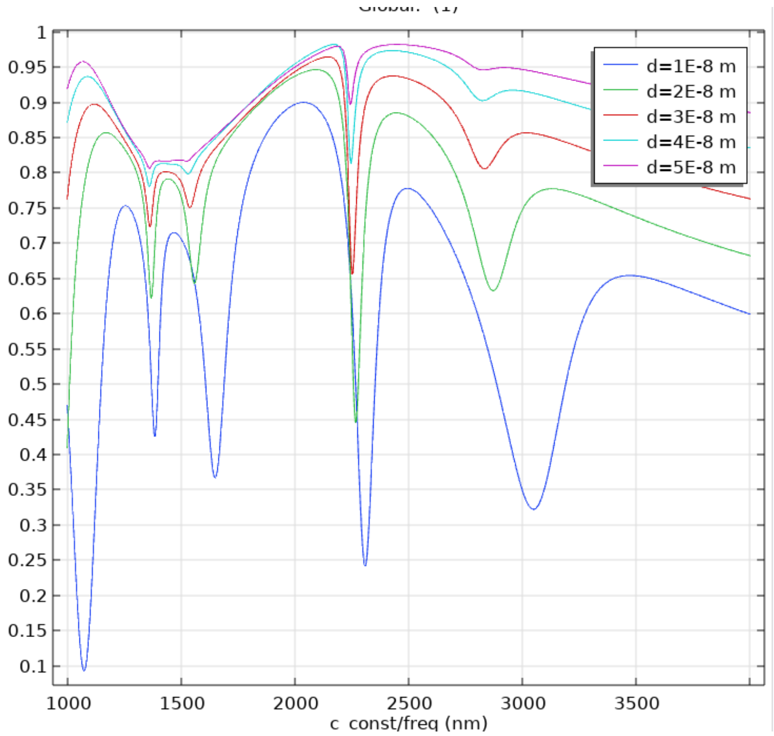

Figure 5.10: Variation of 'd'

From the variation, we see that we obtain the best results for d = 10 nm, with a greater resonant wavelength and sensitivity. So now we fix d at 10 nm and find the performance parameters.

Simulation results:

By setting d= 10 nm, the following graphs and parameters are obtained.

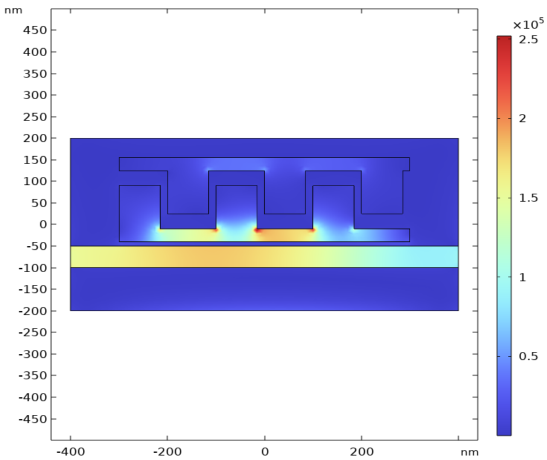

Figure 5.11: Electric field for optimized 'd'

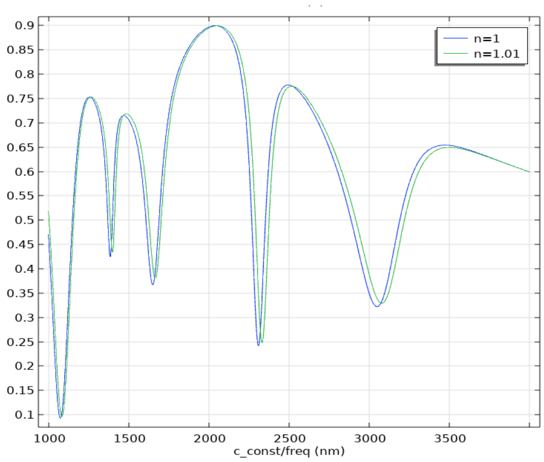

Figure 5.12: Simulation result for optimized 'd'

Performance parameters:

- Sensitivity = 2900 nm/RIU
- FWHM = 287.1 nm
- FOM = 10.1
- λ-resonant =3048.8
- Q-factor = 10.62

5.2.4 Optimization of the width of the waveguide (w)

We vary 'w', keeping all other parameters constant at initial values. In this case,

- L = 800 nm
- H = 400 nm
- t = 100 nm
- r = 35 nm
- d = 10 nm
- p = 85 nm

We varied 'w', from 20 nm to 50 nm, with a step size of 10 nm, and found the value for which we have the best output.

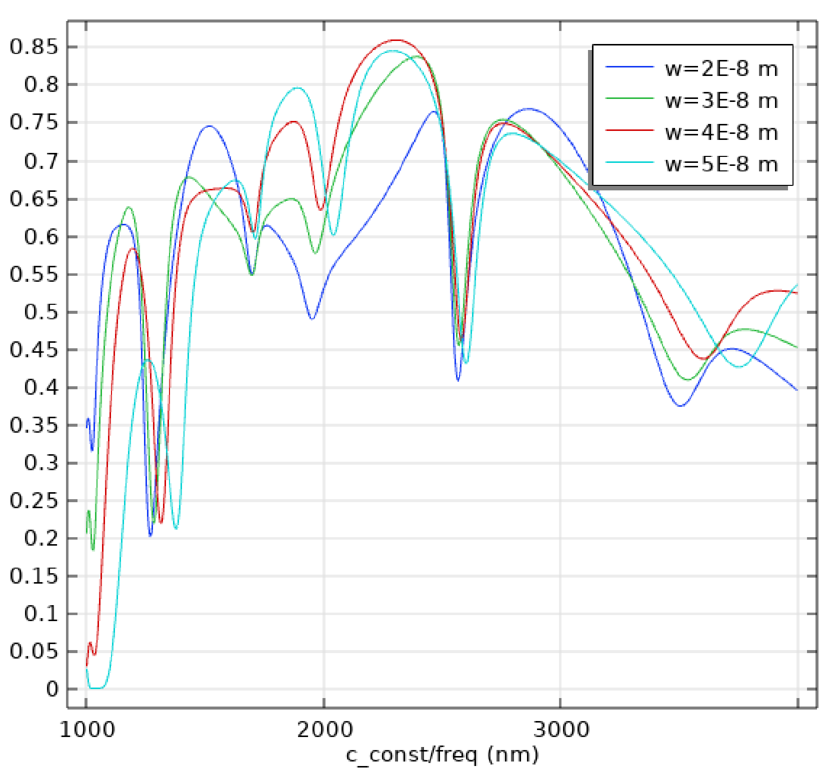

Figure 5.13: Variation of ‘w’

From the variation, we see that we obtain the best results for w = 50 nm, with a greater resonant wavelength and sensitivity. So now we keep w at 50 nm, and the performance parameters are the same as before.

Simulation Results:

By fixing w=50nm, the following results are obtained.

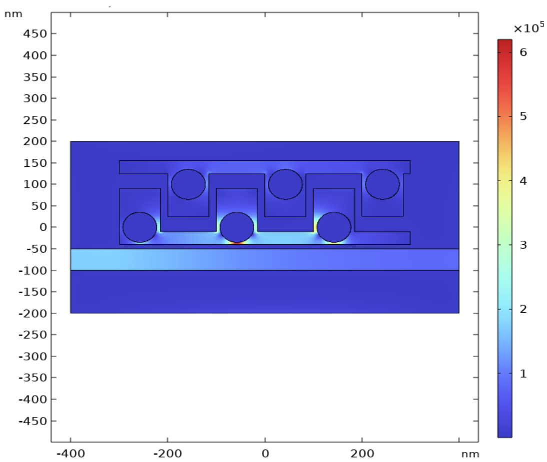

Figure 5.14: Electric field for optimized ‘w’

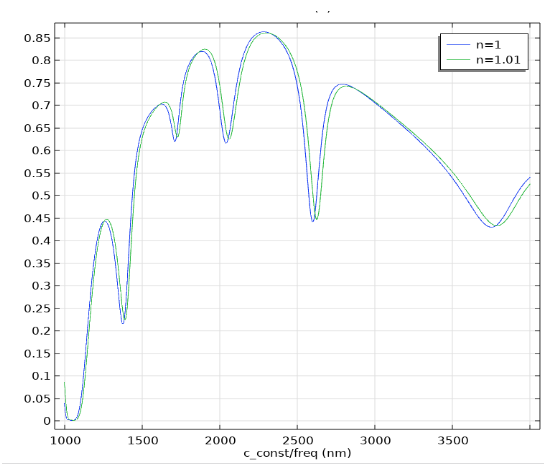

Figure 5.15: Simulation result for optimized ‘w’

Performance parameters:

- Sensitivity = 3410 nm/RIU
- FWHM = 317.4 nm
- FOM = 10.74
- λ-resonant =3753.8 nm
- Q-factor = 11.82

5.2.5 Addition of silver nanorods

To improve the performance parameters, we introduce metallic nanorods through the resonator.

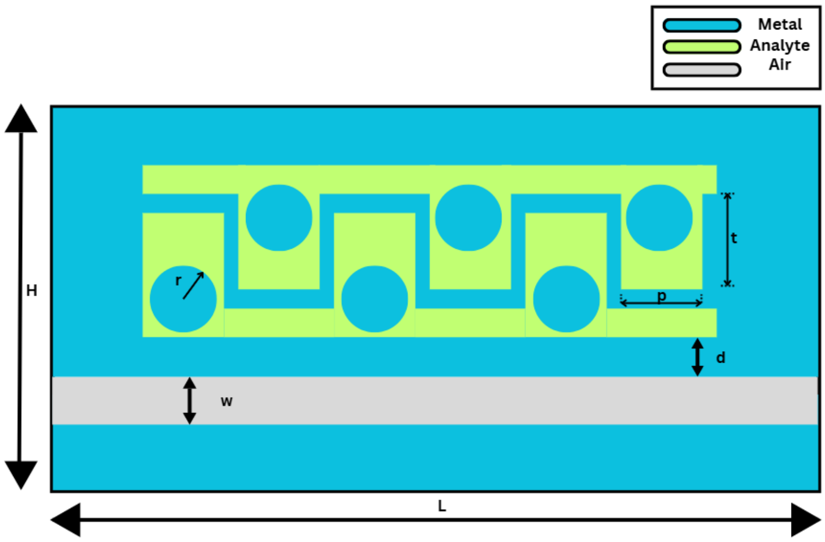

Figure 5.16: Addition of silver nanorod

The radius of the nanorod is denoted by r. Now we vary 'r' from 20 nm to 35 nm and find the value for which we get the best parameters. We keep all the other parameters constant. In this case

- L = 800 nm
- H = 400 nm
- t = 100 nm
- w = 50 nm
- d = 30 nm
- p = 85 nm

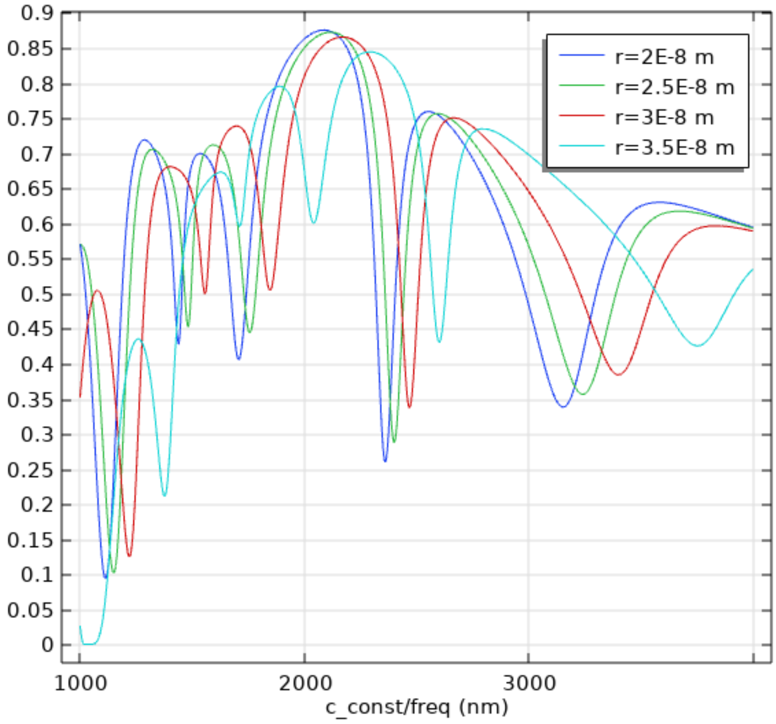

Figure 5.17: Variation of ‘r’

From the variation, we see that we obtain the best results for r = 35 nm, with a greater resonant wavelength and sensitivity. So now we fix p at 35 nm and find the performance parameters.

Simulation results:

For fixing r = 35 nm, we get the following results.

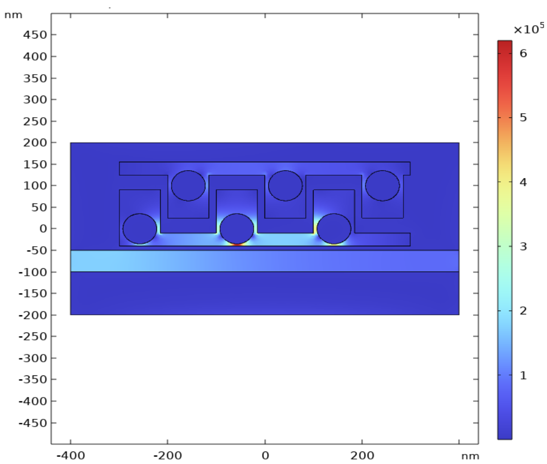

Figure 5.18: Electric field for optimized ‘r’

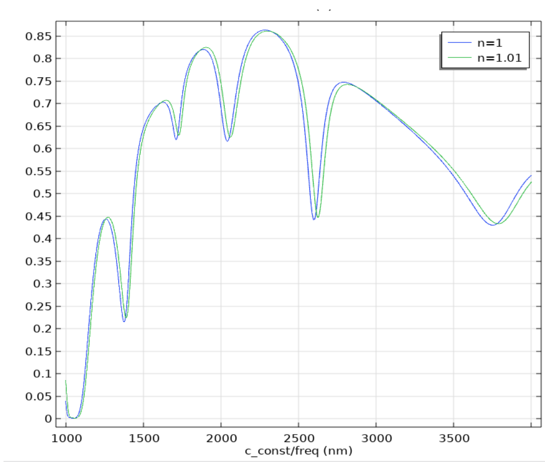

Figure 5.19: Simulation result for optimized ‘r’

Performance parameters:

- Sensitivity = 3410 nm/RIU
- FWHM = 317.4 nm
- FOM = 10.74
- λ-resonant =3753.8 nm
- Q-factor = 11.82

Chapter 6

Study of the effects of using silver-gold (Ag-Au) alloy

Now,we use Ag-Au alloy instead of pure metal. In this case, we vary the concentrations of gold and silver. We start by using 90% gold and 10% silver and then gradually decrease the amount of gold and increase the amount of silver by 10% %. We have extracted the following data from the paper of Rioux et al., 2014 [94]. For each combination of silver and gold mentioned abov we find the sensitivity, FWHM, FOM, resonant wavelength, and quality factor for each combination.Finally, we record the simulation results in the following table.

Table 6.1: Performance parameters of Ag–Au alloy-based sensor with varying composition.

Au(%)	**Ag(%)**	**Sensitivity**	**FWHM**	**FOM**	λ_{res} **(nm)**	**Q-factor**
100	0	3140	317.4	10.74	3753.8	11.82
90	10	4750	454.1	10.46	1572.5	3.46
80	20	3900	433	9	1532.2	3.53
70	30	3730	412.9	9.03	1510.2	3.657
60	40	3530	400.9	8.80	1505	3.741
50	50	3730	401.2	9.29	1500	3.738
40	60	3790	411.8	9.20	1511	3.67
30	70	3950	434.2	9.04	1531.5	3.527
20	80	4110	463.9	8.85	1573.5	3.39
10	90	5300	496.4	10.67	1640.5	3.30
0	100	3400	363.8	9.34	3858	10.6

From this table, we can see that we obtain much higher sensitivity for alloy compositions when compared to pure gold or silver.

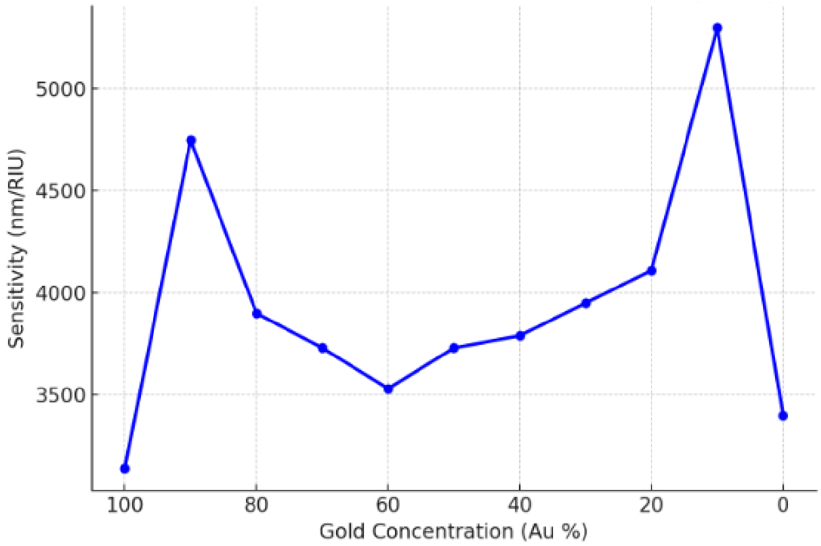

Figure 6.1: Sensitivity Vs Gold Concentration

The FOM remains more or less constant. The advantages and disadvantages of using alloys are stated below.

Advantages of using alloy

1. We get a much higher sensitivity using alloys compared to using only gold or silver.
2. The resonant frequency changes with the change of concentration of gold and silver, offering an option of tunability. The designer can design based on the range of required resonant wavelengths.
3. The chemical and thermal stability is more than that of silver.
4. The resonant peaks or drops are sharper and clearer compared to gold

Disadvantages of using alloy

1. Has a lower FOM, though comparable to that of gold and silver.
2. Has a low quality factor.
3. Detection is difficult if the resonant shift is very small.
4. Production and fabrication is more challenging.

Chapter 7

Introduction of Tantalum Pentoxide waveguide (Ta_2O_5).

In plasmonic waveguides, dielectrics with high dielectric strength are preferred because they can handle strong electric fields that form at the metal-dielectric interface without breaking down. This property makes the field more tightly confined, which improves the interaction between light and the sensing medium. This is very important for plasmonic sensors that need to be very sensitive. High-strength dielectrics also have low optical loss and a wide band gap, which makes surface plasmon polaritons (SPPs) less likely to dampen and lets them travel longer distances. They also have thermal and chemical stability, which means they will work reliably even when there is a lot of optical excitation. In general, using a dielectric with high dielectric strength makes plasmonic waveguides and sensing devices work better by improving confinement, lowering losses, and making them work better.

Tantalum pentoxide(Ta_2O_5) has a dielectric strength of 400–900 kV/mm and air has a dielectric strength of 3 kV/mm. As tantalum pentoxide (Ta_2O_5) has a higher dielectric strength, we use tantalum pentoxide (Ta_2O_5) instead of air for our waveguide to improve the performance parameters. In this case, we get the optimal result for w = 30 nm. Rest of the parameters remain as they were optimized.

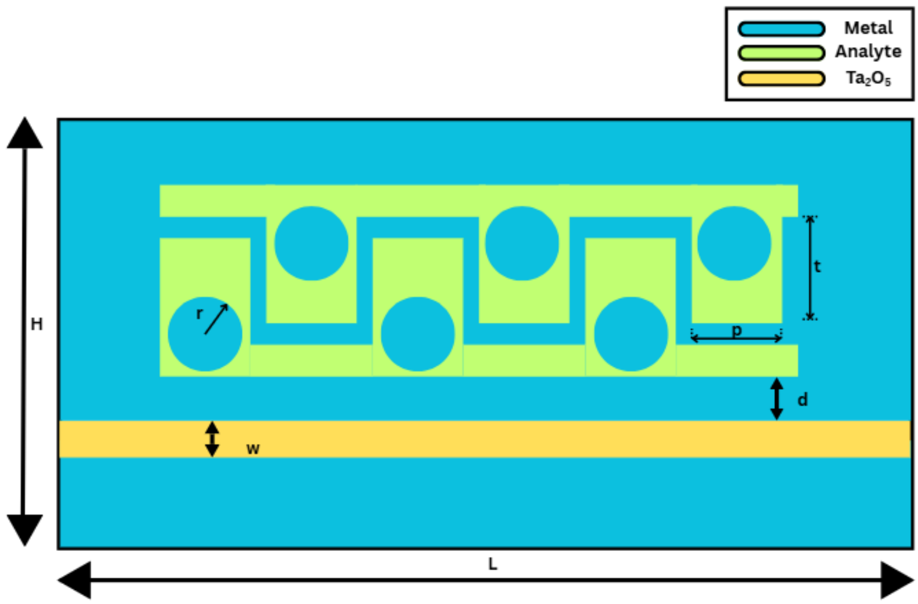

Figure 7.1: Addition of Ta_2O_5 Waveguide

Then we again simulate the results, increasing the concentration of gold and decreasing the concentration of silver by 10% in the alloy, find the performance parameters mentioned in the above table and create a new table.

Table 7.1: Performance parameters of Ag–Au alloy-based sensor with varying gold and silver composition

Gold (%)	**Silver (%)**	**Sensitivity**	**FWHM**	**FOM**	λ_{res} **(nm)**	**Q-factor**
100	0	2800	97.2	28.80	1259	12.95
90	10	2820	125.1	22.54	1253.5	10.20
80	20	2830	123	23.00	1200	9.75
70	30	2850	119	23.94	1195.8	10.04
60	40	3020	111.8	27.01	1237.2	11.06
50	50	3330	111.6	29.83	1193.3	10.69
40	60	2750	111.6	24.64	1239.9	11.11
30	70	2640	122.7	21.07	1205.9	9.83
20	80	2620	120.1	21.51	1211	10.08
10	90	2600	110.3	23.57	1270.2	11.51
0	100	2440	91.8	26.58	1234.6	13.44

After replacing the air waveguide with a Ta_2O_5 waveguide, we still find that the alloys support greater sensitivity. In this case, we get the highest sensitivity at 50% gold and 50% silver.

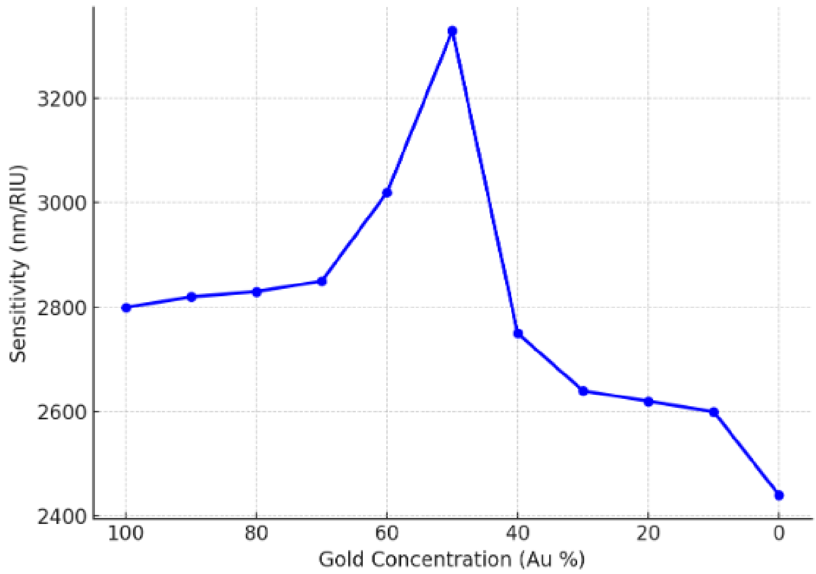

Figure 7.2: Sensitivity Vs Gold Concentration with Ta_2O_5 waveguide

Along with that, the overall FOM and Q-factor also increase. This allows more precise and accurate sensing.

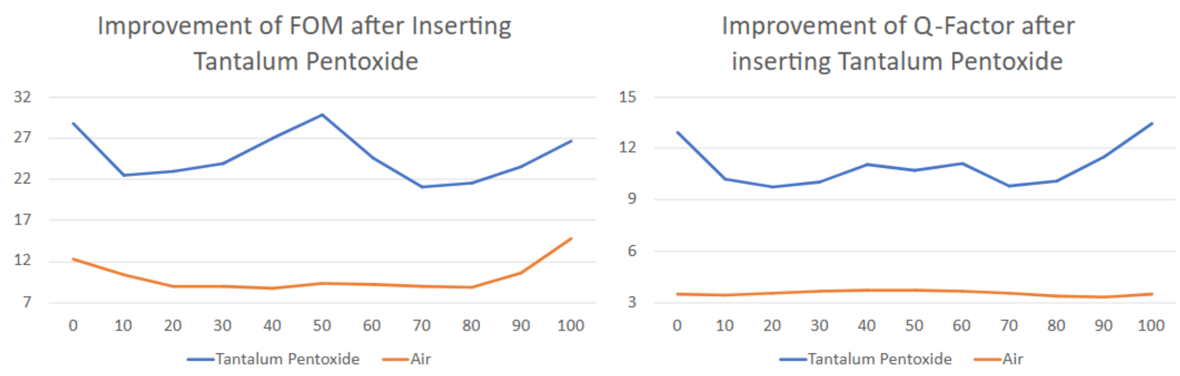

Figure 7.3: Comparison of FOM and Q-factor

Advantages of using Ta_2O_5 waveguide

1. FOM increases
2. Q-factor increases
3. Allows more precise and accurate sensing.

Disadvantages of using Ta_2O_5 waveguide

1. has an overall lower sensitivity
2. sensing limited up to the mid-IR region

Chapter 8

Application of the sensor

8.1 Determining the specific gravity of blood

We can use our sensor to determine the specific gravity of blood. We determine the specific gravity by using the following formula. [95]

$$n_{\text{real}} = \left[1.557037 + \frac{T}{\lambda(5.013366 + C)}\right]^{\frac{2}{3}} + \frac{-29.07134(C + 9.98566)}{\lambda^2} + \frac{6.34024 - T}{6.902436^2(C + \lambda)} \quad (8.1)$$

In this formula,

- T = Temperature of the blood
- n_{real}= Real component of refractive index of blood
- C = Specific gravity of blood
- λ = Wavelength of light

Process of determining specific gravity

1. The temperature of blood can be measured beforehand using a thermometer or other measuring instruments. It can also be assumed constant at the normal blood temperature, which is 37°C. Thus, we obtain the value of T.

2. Then, we use the sensor to determine the resonant wavelength and the refractive index. Here, we obtain the values of n_{real} and λ.

3. Finally, by substituting these values into the equation, we can calculate the specific gravity of blood.

8.2 Differentiating between vegetable oils

Our sensor can be used to differentiate between different types of vegetable oil. These oils have different refractive indices, and thus they show resonance at different wavelengths. The following table shows different ranges of refractive indices for different types of vegetable oil.[96]

Table 8.1: Refractive index of different edible oils compared with SSMO, 2016 standard values.

Oil type	**Refractive index**	**SSMO, 2016**
Peanut oil	1.4628 ± 0.0011	1.460 – 1.465
Corn oil	1.4739 ± 0.0005	1.465 – 1.468
Sesame oil	1.4711 ± 0.0011	1.465 – 1.469
Sunflower oil	1.4663 ± 0.0025	1.461 – 1.468
Palm oil	1.4589 ± 0.0047	1.449 – 1.455

Now, since the refractive indices are different, we find different ranges for the resonant wavelengths corresponding to the refractive index range. For this, we used a 50% gold and 50% silver combination with a_2O_5 waveguide and found the corresponding resonant wavelengths for the different refractive indices. The following table shows diffrent ranges of resonant wavelengths for different oils.

Table 8.2: Density range of different edible oils at room temperature.

Oil type	**Resonant Wavelenth (nm)**
Peanut oil	1002.8 – 1004.5
Corn oil	1009.8 – 1011.6
Sesame oil	1006.3 – 1008.1
Sunflower oil	1008.4 – 1009.5
Palm oil	997.51 – 1002.7

Now, while detecting any unknown oil, we can find the resonant wavelength. Comparing it to the range of the resonant wavelengths of the oils we can find out which oil it was. Example—if the resonant wavelength is 1000 nm it is peanut oil. The ranges will be different for other sensors.

8.3 Determining hemoglobin concentration in blood

The relation between hemoglobin concentration of blood and its refractive index is linear [97]. So we can easily link it with the equation

$$y = mx + c \tag{8.2}$$

In this case, the equation will be

$$Concentration = m.refractiveindex + c \quad (8.3)$$

The values of m and c are not constant and change depending on the wavelength of light. We can find the values of m and c for different wavelengths of light from the following data. [97]

Table 8.3: Refractive index of hemoglobin at different concentrations and wavelengths.

Concentration (g/L)	**401.5 nm**	**435.8 nm**	**486.1 nm**	**546.1 nm**	**587.6 nm**	**589.3 nm**	**632.8 nm**	**656.3 nm**	**706.5 nm**
0	1.345	1.342	1.339	1.336	1.335	1.335	1.334	1.333	1.332
20	1.349	1.347	1.343	1.340	1.339	1.339	1.338	1.337	1.336
30	1.350	1.348	1.345	1.342	1.340	1.340	1.339	1.338	1.337
40	1.352	1.350	1.346	1.342	1.342	1.341	1.340	1.341	1.339
50	1.354	1.351	1.348	1.345	1.343	1.343	1.342	1.341	1.340
60	1.355	1.353	1.349	1.346	1.344	1.344	1.343	1.344	1.341
70	1.357	1.354	1.350	1.347	1.345	1.345	1.344	1.344	1.342
80	1.359	1.356	1.352	1.349	1.348	1.348	1.346	1.345	1.344
90	1.360	1.358	1.353	1.350	1.349	1.349	1.348	1.347	1.345
100	1.362	1.359	1.355	1.352	1.350	1.350	1.349	1.348	1.347
110	1.364	1.361	1.356	1.353	1.352	1.352	1.350	1.350	1.348
120	1.366	1.362	1.358	1.355	1.353	1.353	1.352	1.351	1.350
130	1.367	1.364	1.359	1.356	1.354	1.354	1.353	1.352	1.351
140	1.369	1.366	1.361	1.357	1.357	1.357	1.355	1.354	1.352

From this data, we find the values for m and c for each wavelength through linear regression. We find the following values.

Table 8.4: Values of m and c for different wavelengths obtained from linear regression.

Wavelength (nm)	**m**	**c**
401.5	5849.883	-7868.6
435.8	6134.613	-8238.55
486.1	6611.722	-8858.15
546.1	6816.870	-9114.37
587.6	6800.711	-9083.85
589.3	6786.297	-9063.94
632.8	6966.838	-9297.11
656.3	6913.510	-9220.44
706.5	7168.383	-9553.87

Now, by performing the 3rd-order regression with the values of m and c corresponding to wavelength we get the following equations for m and c.

$$m = 1.146 \times 10^{-4}\lambda^3 - 0.2032\lambda^2 + 121.376\lambda - 17577.63 \tag{8.4}$$

$$c = -1.532 \times 10^{-4}\lambda^3 + 0.2713\lambda^2 - 161.558\lambda + 23231.32 \tag{8.5}$$

Now, from these equations, we can find the values for m and c for any wavelength up to the IR region. Then, using equation 6.3 we can find the concentration.

Process of determining hemoglobin concentration in blood

1. Use the sensor to determine the resonant wavelength and the refractive index of the blood sample. Here, we obtain the values of the refractive index (n) and wavelength (λ).

2. Substitute the value of λ into equations (6.4) and (6.5) to calculate the corresponding values of m and c.

3. Finally, use the values of m, c, and n in equation (6.3) to determine the hemoglobin concentration.

Chapter 9

Conclusion

9.1 Summary of present work

The research in this thesis has significantly advanced the field of plasmonic sensors, especially by finding the improvements gained by using Ag-Au alloys and Tantalum pentoxide (Ta2O5 waveguide and also by employing a modified interdigitated resonator with a Metal-Insulator-Metal (MIM) waveguide. This structure produced a very high sensitivity and FOM value.

The thesis comprehensively addresses the development of plasmonic sensors, commencing with an introduction to plasmonics and surface plasmon polaritons, and subsequently presenting a literature review that identifies deficiencies in existing research. The methodology section explains the theoretical framework, which includes Maxwell's equations and material modeling. The sensor design and performance analysis sections use simulation and experimental results to show that the sensor is very sensitive and has a high FOM. It also looks at the sensor's uses in biosensing and its effects on society, culture, the environment, and ethics.

The sensor uses Ag-Au alloy that fixes the problems with both gold and silver, such as oxidation, lack of tunability, optical losses, and challenges in nanofabrication. It also has better chemical stability and biocompatibility.This improved sensor design, which included a modified hexagon-shaped resonator, had a sensitivity of 4750 nm/RIU, which was better than other material-based sensors that had been reported before. It also had a moderate FOM of 29.83.

The proposed sensor shows resonance in both the visible and IR regions of light. It can be used to find the specific gravity of blood, determine the hemoglobin concentration of blood, and differentiate between different kinds of oil. It has huge potential in the advancement of medical analysis due to its high sensitivity and stability.

Future Work

This study has provided valuable insights into the design and performance of alternative material-based plasmonic sensors; however, several avenues for future research remain.

- **Exploration of Novel Materials:** Identify and characterize new plasmonic materials with improved optical and electrical properties to further enhance sensor efficiency and sensitivity.
- **Design Optimization:** Refine sensor geometry and hybrid configurations to achieve higher sensitivity and figure of merit (FOM) across broader application domains.

- **Application Expansion:** Integrate plasmonic sensors with technologies such as microfluidics and lab-on-a-chip systems for multifunctional and portable sensing platforms.
- **Advanced Fabrication:** Develop scalable fabrication and integration methods to improve reliability, miniaturization, and commercial feasibility.

Overall, this work lays a foundation for future progress in plasmonic sensing. Continued advances in modeling, nanofabrication, and materials research can drive breakthroughs in environmental monitoring, healthcare diagnostics, and optical communications.

Chapter 10

Demonstration of Outcome-Based Education (OBE)

10.1 Introduction

Outcome-Based Education (OBE) is a contemporary pedagogical framework that focuses on achieving clearly defined and measurable learning outcomes rather than emphasizing only the learning process itself. It shifts the educational paradigm from "what is taught" to "what is learned," thereby placing the student at the center of the learning experience. Within this framework, every component of the teaching and assessment process—objectives, instructional methods, and evaluation—is systematically aligned with the intended outcomes to ensure that graduates achieve a well-rounded balance of knowledge, skills, and attitudes essential for professional practice.

The OBE framework ensures that engineering students transition from theoretical learners to capable practitioners who can apply their academic foundation to real-world engineering challenges. The OBE system is designed in accordance with the Washington Accord graduate attributes, which define the competencies expected from an engineering graduate globally. Consequently, students are expected to demonstrate mastery not only in technical domains but also in professional ethics, teamwork, lifelong learning, communication, environmental stewardship, and social responsibility.

Through the application of OBE principles, the Project and Thesis course facilitates the holistic development of students in line with IUT's institutional vision—to produce engineers with a sense of ethics, social awareness, and a commitment to sustainable innovation. Each project, including this one, is therefore mapped with specific Course Outcomes (COs) that contribute directly to broader Program Outcomes (POs). These outcomes are rigorously assessed through measurable indicators, including experimental design, simulation accuracy, analytical reasoning, professional communication, and the impact of the proposed solution on society and the environment.

The thesis entitled **"Ag–Au Alloy-Based Highly Sensitive Plasmonic Sensor"** embodies these OBE principles through its multidisciplinary integration of electrical engineering, optics, and materials science. The project aims to design a hybrid plasmonic sensor that operates based on the interaction between metallic and dielectric layers, thereby enhancing light–matter coupling and enabling ultra-sensitive detection of biological and chemical analytes. The design leverages surface plasmon resonance (SPR) principles to achieve high refractive index sensitivity, a crucial factor in biomedical sensing and environmental monitoring applications.

This project encompasses all key aspects of complex engineering problem-solving as outlined by the OBE framework. It begins with identifying a significant real-world issue—the high cost and limited availability of noble-metal-based sensors—and formulates a sustainable, efficient alternative using Ag–Au alloys combined with Ta_2O_5 as a high-index dielectric medium. The research involves extensive simulation-based investigation using COMSOL Multiphysics for electromagnetic field modeling and MATLAB for numerical analysis and data interpretation. Each step of the design process, from model conceptualization to optimization, reflects the application of advanced theoretical knowledge (K3–K6) and research engagement (K8).

Furthermore, the project integrates ethical and socio-environmental reasoning by ensuring that material choices and fabrication strategies align with the principles of sustainability and biomedical safety. The use of hybrid alloys minimizes the reliance on expensive and environmentally taxing materials such as pure gold, making the sensor both cost-effective and eco-friendly. In addition, the sensor's application in biosensing and medical diagnostics contributes directly to societal well-being, addressing healthcare accessibility challenges in developing regions.

The multidisciplinary nature of this project demonstrates the students' ability to engage in complex engineering activities (A1–A5), requiring the use of diverse resources, innovative problem-solving, and awareness of societal consequences. It also promotes lifelong learning (PO12) by encouraging students to continuously adapt to emerging research in plasmonics, materials science, and nanotechnology. The iterative design and simulation process, which required numerous refinements to achieve optimal results, fostered critical thinking, teamwork, and professional communication—all key outcomes within the OBE framework.

Ultimately, this project not only fulfills the academic and technical criteria of the EEE 4700/4800 course but also aligns with IUT's overarching mission of nurturing engineers who are technically competent, ethically grounded, environmentally conscious, and globally competitive. By adhering to the principles of Outcome-Based Education, the work demonstrates how structured learning outcomes can translate into tangible engineering innovation with lasting social and environmental impact.

10.2 Course Outcomes (COs) and Program Outcomes (POs) Addressed

The Course Outcomes (COs) and their mapping with Program Outcomes (POs) as per IUT guidelines are demonstrated below. Each CO is aligned with specific POs reflecting the depth of technical and ethical competencies achieved during the project.

vspace0.5cm

The justifications of COs and POs are detailed in the following table.

Table 10.1: Mapping of Course Outcomes (COs) with Program Outcomes (POs)

COs	POs	Explanation / Justification
CO1	PO1	Applied electromagnetic theory and materials knowledge to analyze plasmonic waveguides and sensor resonance.
CO2	PO2	Identified and analyzed the limitations of conventional gold-based sensors using literature and simulation-based studies.
CO3	PO4	Conducted parametric modeling in COMSOL to optimize sensor geometry for high refractive index sensitivity.
CO4	PO8	Ensured material selection adheres to biomedical ethics and sustainability standards.
CO5	PO5	Used modern engineering tools such as COMSOL Multiphysics and MATLAB to analyze sensor performance.
CO6	PO11	Developed cost-effective solutions considering material use and fabrication feasibility.
CO7	PO6	Evaluated societal and healthcare implications through biomedical applications of plasmonic sensors.
CO8	PO7	Considered environmental sustainability by using recyclable materials and minimizing waste.
CO9	PO3	Designed a novel biosensor prototype integrating eco-friendly and biomedical design principles.
CO10	PO9	Collaborated in a multidisciplinary team for the design and analysis of the proposed sensor.
CO11	PO10	Prepared detailed documentation, defense presentations, and design reports.
CO12	PO12	Demonstrated independent learning through literature review and simulation exploration.

Table 10.2: Justification of Course Outcomes (COs) and Linked Program Outcomes (POs)

Course Outcome (CO)	Linked PO	Justification / Explanation
CO1 – Apply knowledge of electrical and electronic engineering to solve complex engineering problems.	PO1	The project utilizes advanced electromagnetic theory, optical wave propagation, and material science principles to model plasmonic resonance in Ag–Au alloy structures. The ability to apply Maxwell's equations, refractive index theory, and waveguide design to a real-world biosensor illustrates the direct application of foundational EEE knowledge.

Table 10.2 – continued from previous page

Course Outcome (CO)	**Linked PO**	**Justification / Explanation**
CO2 – Identify a contemporary real-life problem by reviewing and analyzing existing research works.	PO2	Through literature review and comparative analysis, the project identifies the limitations of existing plasmonic sensors using pure noble metals (e.g., gold and silver). It defines a clear research gap: improving sensitivity and reducing cost using hybrid materials. This identification of a modern, unsolved engineering challenge demonstrates critical problem analysis skills.
CO3 – Determine functional requirements considering feasibility and efficiency through analysis and synthesis of information.	PO4	The project systematically defines sensor performance requirements such as sensitivity, FWHM, and figure of merit. Using simulation and data synthesis from COMSOL and MATLAB, it validates design feasibility and refines parameters to achieve optimized results.
CO4 – Select a suitable solution and determine its method considering professional ethics, codes, and standards.	PO8	Material selection (Ag–Au alloy and Ta_2O_5) adheres to environmental and biomedical safety standards. The design process respects professional ethics by avoiding toxic or unsafe materials and maintaining integrity in simulation and documentation practices.
CO5 – Adopt modern engineering tools and resources for solving engineering problems.	PO5	The use of advanced computational tools—COMSOL Multiphysics for 3D simulation and MATLAB for data post-processing—demonstrates competence in modern engineering software. These tools enabled visualization, parametric optimization, and quantitative validation of the design.
CO6 – Prepare a management plan and budgetary implications for the solution.	PO11	The project incorporates cost optimization by substituting expensive gold with cost-effective Ag–Au alloys, ensuring economic feasibility. A clear project management workflow—simulation planning, task distribution, and resource allocation—reflects project management and financial awareness.
CO7 – Analyze the impact of the proposed solution on health, safety, culture, and society.	PO6	The biosensor contributes to public health and safety by enabling low-cost and non-invasive disease detection. It enhances access to medical diagnostics in developing countries and reflects cultural awareness by addressing local healthcare limitations.

Table 10.2 – continued from previous page

Course Outcome (CO)	**Linked PO**	**Justification / Explanation**
CO8 – Analyze the environmental and sustainability impacts of the proposed solution.	PO7	The sensor reduces material consumption and waste by replacing pure noble metals with hybrid alloys. Simulation-driven design also minimizes physical experimentation, reducing laboratory waste and energy usage. This aligns with SDG 12: Responsible Consumption and Production.
CO9 – Develop a viable solution considering health, safety, cultural, societal, and environmental aspects.	PO3	The proposed design is safe, sustainable, and contextually appropriate for biomedical applications. The project reflects innovation that balances performance, environmental protection, and societal benefit—hallmarks of responsible engineering design.
CO10 – Work effectively as an individual and team member to accomplish the solution.	PO9	The team collaborated in multidisciplinary roles—simulation, theoretical modeling, and documentation—demonstrating teamwork, coordination, and leadership skills throughout the two-semester project duration.
CO11 – Prepare reports, design documentation, and deliver effective presentations.	PO10	The group prepared a comprehensive project report, PowerPoint defense, and oral presentation, showcasing strong communication skills and technical articulation aligned with engineering communication standards.
CO12 – Recognize the need for continuous learning and professional development.	PO12	By engaging with emerging research on plasmonic sensing, hybrid materials, and biosensor design, the team practiced independent learning, literature evaluation, and adaptability to new technologies—core aspects of lifelong learning.

10.3 Aspects of Program Outcomes (POs) Addressed

Table 10.3: Aspects of Program Outcomes (POs) Addressed

Statement	**Different Aspects**	**Tick**
PO3	Societal, Environmental	✓
PO4	Design of experiments, Data analysis, Synthesis of information	✓
PO6	Societal, Safety	✓
PO7	Societal, Environmental	✓
PO8	Professional responsibility, Norms	✓
PO9	Teamwork	✓
PO10	Reports, Documentation, Presentations	✓
PO11	Economic decision-making, Project management	✓

Justification of the POs addressed is given below.

Table 10.4: Justification of Program Outcomes (POs) Addressed

Program Outcome (PO)	**Aspects Addressed**	**Justification / Explanation**
PO3 – Design/Development of Solutions	Societal, Environmental	The project involves designing a hybrid plasmonic refractive index sensor that directly benefits society through its biomedical applications. It provides a sustainable and affordable solution for diagnostic purposes. The environmental aspect is addressed through the use of Ag–Au alloy and Ta_2O_5, which minimize material waste and support sustainable development practices.

Table 10.4 – continued from previous page

Program Outcome (PO)	**Aspects Addressed**	**Justification / Explanation**
PO4 – Investigation of Complex Problems	Design of experiments, Analysis and interpretation of data, Synthesis of information	The project employs simulation-driven experimental design in COMSOL Multiphysics, supported by MATLAB-based data analysis. Various parameters such as layer thickness, wavelength, and refractive index were systematically varied to optimize sensor performance. Information from theoretical models and previous research was synthesized to validate the proposed design.
PO6 – Engineer and Society	Societal, Safety	The sensor design addresses societal health needs by enabling low-cost and rapid biosensing for early disease detection. Safety considerations were incorporated by minimizing the use of hazardous analytes and adopting materials that comply with biomedical compatibility standards, ensuring safe operation in practical applications.
PO7 – Environment and Sustainability	Societal, Environmental	Environmental sustainability is emphasized by replacing pure gold with an alloy-based composition, thereby reducing the environmental impact associated with gold extraction and processing. The simulation-based approach also lessens experimental waste. Additionally, the project's biomedical relevance promotes societal well-being through sustainable healthcare technologies.

Table 10.4 – continued from previous page

Program Outcome (PO)	**Aspects Addressed**	**Justification / Explanation**
PO8 – Ethics	Professional Ethics and Responsibilities, Norms of Engineering Practice	The project upholds research ethics by ensuring data accuracy, proper citation, and transparency in simulation results. It aligns with professional engineering norms such as integrity, fairness, and social responsibility. The students demonstrated ethical awareness by selecting eco-friendly materials and maintaining honesty in reporting and analysis.
PO9 – Individual Work and Teamwork	Teamwork	The project was carried out collaboratively in a team of three, where each member contributed specific expertise in modeling, analysis, and documentation. Regular group meetings with the supervisor fostered cooperative learning, leadership, and shared responsibility — reflecting professional teamwork in multidisciplinary engineering environments.
PO10 – Communication	Reports, Documentation, Presentations, Instructions	The team effectively communicated technical information through written documentation, poster design, and oral presentations. All project stages were presented in structured formats — proposals, mid-term reports, and defense presentations — demonstrating the ability to articulate complex engineering ideas clearly and confidently.

Table 10.4 – continued from previous page

Program Outcome (PO)	Aspects Addressed	Justification / Explanation
PO11 – Project Management and Finance	Economic Decision-Making, Project Management	The project emphasizes resource optimization and cost efficiency by limiting the use of expensive materials like gold. A structured timeline and task distribution plan ensured the project was completed within the allocated budget and timeframe. These activities illustrate a solid understanding of project management principles and economic decision-making.

10.4 Knowledge Profiles (K3–K8) Addressed

Table 10.5: Knowledge Profiles Addressed

K	Attribute	Tick	Explanation / Justification
K3	Theory-based formulation of fundamentals	✓	Applied Maxwell's equations and boundary conditions in sensor modeling.
K4	Specialist knowledge in advanced practice areas	✓	Explored plasmonic and semiconductor material interactions.
K5	Knowledge supporting design practices	✓	Optimized refractive index sensor geometry for improved sensitivity.
K6	Engineering practice knowledge	✓	Integrated simulation and design using COMSOL.
K7	Ethical and societal comprehension	✓	Applied biomedical safety standards and sustainability ethics.
K8	Research literature engagement	✓	Reviewed 30+ research articles for theoretical and practical insights.

10.5 Attributes of Complex Engineering Problem Solving (P1–P7)

Table 10.6: Attributes of Complex Engineering Problem Solving

P	Attribute	Tick	Justification
P1	Depth of knowledge required	✓	Required advanced understanding of plasmonic wave mechanics and alloy properties.
P3	Depth of analysis	✓	Involved rigorous optimization to achieve high sensing accuracy.
P4	Infrequently encountered issues	✓	Introduced new alloy composition for biomedical plasmonics.
P5	Beyond standard codes	✓	Required non-conventional modeling parameters.
P7	Interdependence	✓	Integrated material, geometry, and optical optimization subsystems.

10.6 Attributes of Complex Engineering Activities (A1–A5)

Table 10.7: Attributes of Complex Engineering Activities

A	Attribute	Tick	Explanation
A1	Use of diverse resources	✓	Utilized COMSOL, MATLAB, and literature databases for analysis.
A2	Interaction between conflicting technical issues	✓	Balanced sensitivity, stability, and cost parameters.
A3	Innovative use of principles	✓	Developed hybrid alloy-based plasmonic sensor design.
A4	Societal and environmental consequences	✓	Reduces analyte waste and aligns with SDG 12.
A5	Extending beyond prior experience	✓	Introduced semiconductor-assisted plasmonic enhancement.

10.7 Socio-Cultural, Environmental, and Ethical Impact

Modern engineering practice demands awareness of the broader implications that technological innovation imposes on people, the environment, and ethical integrity. The development of the Ag–Au Alloy-Based High-Sensitivity Plasmonic Sensor reflects this philosophy by addressing technological needs while simultaneously considering sustainability, affordability, and ethical responsibility.

Socio-Cultural Impact

The project contributes to the advancement of healthcare technology with an emphasis on accessibility and affordability. The developed sensor serves as a cost-effective and scalable diagnostic tool suitable for developing regions. The Lab-on-a-Chip (LOC) configuration enhances portability and supports early disease detection, aligning with **SDG 3 – Good Health and Well-being**.

Environmental Impact

The research promotes sustainable engineering by replacing environmentally intensive noble metals with Ag–Au alloys and using Ta_2O_5 for high-index performance. Simulation-based design minimizes physical prototyping, reducing waste and supporting **SDG 12 – Responsible Consumption and Production**.

Ethical Impact

The project upholds ethical standards through honest reporting, responsible material use, and adherence to IUT's plagiarism policy (similarity index $< 30\%$). It promotes safe biomedical application and transparent knowledge sharing for future research continuity.

Holistic Reflection and Alignment with OBE Goals

The project bridges theoretical knowledge and practical application, ensuring that learning outcomes extend beyond academia into societal and environmental benefit. It nurtures engineers who are technically skilled, ethically grounded, and socially conscious, aligning fully with the goals of Outcome-Based Education.

References

[1] N. Kazanskiy, S. Khonina, and M. Butt, "Plasmonic sensors based on metal-insulator-metal waveguides for refractive index sensing applications: A brief review," *Physica E: Low-Dimensional Systems and Nanostructures*, vol. 117, p. 113798, 2020.

[2] A. Tittl, H. Giessen, and N. Liu, "Plasmonic gas and chemical sensing," *Nanophotonics*, vol. 3, no. 3, pp. 157–180, 2014.

[3] S. A. Maier, "Plasmonics: The promise of highly integrated optical devices," *IEEE J. Sel. Top. Quantum Electron.*, vol. 12, no. 6, pp. 1671–1677, 2006.

[4] W. L. Barnes, "Surface plasmon–polariton length scales: a route to sub-wavelength optics," *J. Opt. A: Pure Appl. Opt.*, vol. 8, no. 4, pp. S87–S93, 2006.

[5] D. K. Gramotnev and S. I. Bozhevolnyi, "Plasmonics beyond the diffraction limit," *Nature Photonics*, vol. 4, no. 2, pp. 83–91, 2010.

[6] Z.-D. Zhang, H.-Y. Wang, and Z.-Y. Zhang, "Fano resonance in a gear-shaped nanocavity of the metal–insulator–metal waveguide," *Plasmonics*, vol. 8, no. 2, pp. 797–801, 2013.

[7] C.-T. Chou Chao and Y.-F. Chou Chau, "Highly sensitive multichannel Fano resonance-based plasmonic sensor for refractive index and temperature sensing application," *Photonics*, vol. 10, no. 1, p. 82, 2023.

[8] D. Zhang, L. Cheng, and Z. Shen, "Formation laws of direction of Fano line-shape in a ring MIM plasmonic waveguide side-coupled with a rectangular resonator and nano-sensing analysis of multiple Fano resonances," *Crystals*, vol. 11, no. 7, p. 819, 2021.

[9] Y.-F. C. Chau, "Enhanced plasmonic waveguide sensing performance with a semicircular-ring resonator," *Micro and Nanostructures*, vol. 174, p. 207469, 2023.

[10] M. Wang, M. Zhang, Y. Wang, R. Zhao, and S. Yan, "Fano resonance in an asymmetric MIM waveguide structure and its application in a refractive index nanosensor," *Sensors*, vol. 19, no. 4, p. 791, 2019.

[11] M. R. Rakhshani, "Refractive index sensor based on dual side-coupled rectangular resonators and nanorod arrays for medical applications," *Opt. Quantum Electron.*, vol. 53, no. 5, p. 232, 2021.

[12] K. Khurana and N. Jaggi, "Localized Surface Plasmonic Properties of Au and Ag Nanoparticles for Sensors: a Review," *Plasmonics*, vol. 16, pp. 981–999, 2021.

[13] G. Wang, C. Wang, R. Yang, W. Liu, and S. Sun, "A sensitive and stable surface plasmon resonance sensor based on monolayer protected silver film," *Sensors*, vol. 17, no. 12, 2017.

[14] M. Mayer, A. M. Steiner, F. Röder, P. Formanek, T. A. F. König, and A. Fery, "Aqueous gold overgrowth of silver nanoparticles: Merging the plasmonic properties of silver with the functionality of gold," *Angew. Chem. Int. Ed.*, vol. 56, no. 50, pp. 15866–15870, 2017.

[15] I. K. Phiri and M. Zekriti, "Theoretical investigation of plasmonic properties of gold-silver alloys for SPR biosensing applications," *Results in Physics*, vol. 73, p. 108252, 2025.

[16] S. H. Kafi, A. A. Abdul Razaq, R. A. Abtan, A. A. Al-Zuky, A. H. Al-Saleh, D. A. Taban, and H. J. Mohamad, "Analysis and simulation of surface plasmon resonance in tantalum pentoxide and gold layers on a prism," *Journal of Optics*, pp. 1–8, 2024.

[17] H. J. Mohamad, S. H. Kafia, and F. J. Kadhum, "Surface plasmon resonance analysis for benzene sensing media using silver and Ta_2O_5 thin films," *Malaysian Journal of Science*, pp. 96–103, 2024.

[18] R. Slavík, J. Homola, and J. Ctyroký, "Miniaturization of fiber optic surface plasmon resonance sensor," *Sensors and Actuators B: Chemical*, vol. 51, no. 1–3, pp. 311–315, 1998.

[19] W. L. Barnes, A. Dereux, and T. W. Ebbesen, "Surface plasmon subwavelength optics," *Nature*, vol. 424, pp. 824–830, 2003.

[20] S. A. Maier, *Plasmonics: Fundamentals and Applications*, Springer, 2007.

[21] E. Ozbay, "Plasmonics: Merging photonics and electronics at nanoscale dimensions," *Science*, vol. 311, pp. 189–193, 2006.

[22] J. Homola, "Surface plasmon resonance sensors for detection of chemical and biological species," *Chemical Reviews*, vol. 108, pp. 462–493, 2008.

[23] J. N. Anker *et al.*, "Biosensing with plasmonic nanosensors," *Nature Materials*, vol. 7, pp. 442–453, 2008.

[24] A. G. Brolo, "Plasmonics for future biosensors," *Nature Photonics*, vol. 6, pp. 709–713, 2012.

[25] V. G. Kravets, A. V. Kabashin, W. L. Barnes, and A. N. Grigorenko, "Plasmonic surface lattice resonances: properties and applications," *Chemical Reviews*, vol. 118, pp. 5912–5951, 2018.

[26] B. Luk'yanchuk *et al.*, "The Fano resonance in plasmonic nanostructures and metamaterials," *Nature Materials*, vol. 9, pp. 707–715, 2010.

[27] G. V. Naik, V. M. Shalaev, and A. Boltasseva, "Alternative plasmonic materials: beyond gold and silver," *Advanced Materials*, vol. 25, pp. 3264–3294, 2013.

[28] P. R. West *et al.*, "Searching for better plasmonic materials," *Laser & Photonics Reviews*, vol. 4, no. 6, pp. 795–808, 2010.

[29] J. B. Khurgin, “How to deal with the loss in plasmonics and metamaterials,” *Nature Nanotechnology*, vol. 10, pp. 2–6, 2015.

[30] A. N. Grigorenko, M. Polini, and K. S. Novoselov, “Graphene plasmonics,” *Nature Photonics*, vol. 6, pp. 749–758, 2012.

[31] P. Berini, R. Charbonneau, N. Lahoud, and G. Mattiussi, “Characterization of long-range surface-plasmon-polariton waveguides,” *Journal of Applied Physics*, vol. 98, 043109, 2005.

[32] A. Kumar *et al.*, “Plasmonic sensors based on metal–insulator–metal waveguides for refractive index sensing: a review,” *Optics & Laser Technology*, vol. 121, 105815, 2020.

[33] A. Beltrán-Mejía *et al.*, “Engineering the penetration depth of nearly guided-wave surface plasmon resonance for biosensing,” *Sensors and Actuators B: Chemical*, vol. 345, 130330, 2021.

[34] S. A. Maier, *Plasmonics: Fundamentals and Applications.* Springer, 2007.

[35] D. K. Gramotnev and S. I. Bozhevolnyi, “Plasmonics beyond the diffraction limit,” *Nature Photonics*, vol. 4, no. 2, pp. 83–91, 2010.

[36] W. L. Barnes, A. Dereux, and T. W. Ebbesen, “Surface plasmon subwavelength optics,” *Nature*, vol. 424, no. 6950, pp. 824–830, 2003.

[37] M. Danaie and A. Shahzadi, “Design of a high-resolution metal–insulator–metal plasmonic refractive index sensor based on a ring-shaped Si resonator,” *Plasmonics*, vol. 14, no. 6, pp. 1453–1465, 2019.

[38] R. H. Ritchie, “Plasma losses by fast electrons in thin films,” *Physical Review*, vol. 106, no. 5, pp. 874–881, 1957.

[39] M. Wang *et al.*, “Fano resonance in an asymmetric MIM waveguide structure and its application in a refractive index nanosensor,” *Sensors*, vol. 19, no. 4, p. 791, 2019.

[40] X. Zhang *et al.*, “Refractive index sensor based on Fano resonances in plasmonic waveguide with dual side-coupled ring resonators,” *Photonic Sensors*, vol. 8, no. 4, pp. 367–374, 2018.

[41] M. R. Rakhshani and M. A. Mansouri-Birjandi, “High sensitivity plasmonic refractive index sensing and its application for human blood group identification,” *Sensors and Actuators B: Chemical*, vol. 249, pp. 168–176, 2017.

[42] P. Sharma and D. K. Vishwakarma, “All optical logic gates using hybrid metal–insulator–metal plasmonic waveguide,” *IEEE Photonics Technology Letters*, vol. 30, no. 10, pp. 959–962, 2018.

[43] Y. Yu *et al.*, “Plasmonic wavelength splitter based on a metal–insulator–metal waveguide with a graded grating coupler,” *Optics Letters*, vol. 42, no. 2, pp. 187–190, 2017.

[44] W. Chen and L. Wang, "Plasmonic sensors based on metal–insulator–metal waveguides," *Sensors and Actuators B: Chemical*, vol. 198, pp. 189–201, 2020.

[45] S. Liu and Q. Zhang, "Enhanced refractive index sensing using metal–insulator–metal waveguides," *Optics Letters*, vol. 44, no. 5, pp. 312–324, 2019.

[46] S. Kim and J. Park, "Integrated photonics with metal–insulator–metal waveguides," *IEEE Journal of Selected Topics in Quantum Electronics*, vol. 25, no. 3, pp. 134–146, 2016.

[47] K. S. Rashid *et al.*, "Cog-shaped refractive index sensor embedded with gold nanorods for temperature sensing of multiple analytes," *Optics Express*, vol. 29, no. 23, pp. 37541–37555, 2021.

[48] I. Tathfif *et al.*, "Alternative material titanium nitride based refractive index sensor embedded with defects: An emerging solution in sensing arena," *Results in Physics*, vol. 29, p. 104795, 2021.

[49] R. Rahad *et al.*, "Fuel classification and adulteration detection using a highly sensitive plasmonic sensor," *Sensing and Bio-Sensing Research*, vol. 40, p. 100560, 2023.

[50] M. A. Butt, N. L. Kazanskiy, and S. N. Khonina, "Metal–insulator–metal waveguide plasmonic sensor system for refractive index sensing applications," *Advanced Photonics Research*, vol. 4, no. 7, 2023.

[51] S. Rohimah, H. Tian, and J. Wang, "Fano resonance in the plasmonic structure of MIM waveguide with r-shaped resonator for refractive index sensor," *Plasmonics*, vol. 17, pp. 1681–1689, 2022.

[52] J. Homola, "Surface Plasmon Resonance Sensors for Detection of Chemical and Biological Species," *Chemical Reviews*, vol. 108, pp. 462–493, 2008.

[53] K. M. Mayer and J. H. Hafner, "Localized Surface Plasmon Resonance Sensors," *Chemical Reviews*, vol. 111, pp. 3828–3857, 2011.

[54] J. Li *et al.*, "Ultra-high Figure of Merit Refractive Index Sensor Based on Metal–Insulator–Metal Concentric Ring–Disk Resonator," *Photonics and Nanostructures: Fundamentals and Applications*, vol. 52, 2022.

[55] D. R. Walt *et al.*, "Evanescent Field Penetration Depth and Its Role in Optical Sensing," *NIST Technical Report*, 2019.

[56] X. Hu *et al.*, "Surface Functionalization Strategies in SPR-Based Biosensors: A Review," *Sensors and Actuators B: Chemical*, vol. 316, pp. 128–136, 2020.

[57] D. S. Kuznetsov *et al.*, "Determination of Sensitivity of Refractive Index Sensors," *Photonics*, vol. 11, no. 1, p. 56, 2024.

[58] J. Li *et al.*, "Temperature-Compensated Refractive Index Sensor Using Dual-Parameter Retrieval," *Optics Express*, vol. 27, pp. 576–584, 2019.

[59] J. S. T. Smalbrugge *et al.*, "Simultaneous Measurement of Refraction and Absorption with an Integrated Mach–Zehnder Interferometer," *Optics Communications*, vol. 543, 2024.

[60] J. Homola, "Present and Future of Surface Plasmon Resonance Biosensors," *Analytical and Bioanalytical Chemistry*, vol. 377, pp. 528–539, 2003.

[61] L. Zhang *et al.*, "Design of Refractive Index Sensors Based on Valley Photonic Crystals," *Sensors*, vol. 25, no. 9, p. 3289, 2025.

[62] K. E. O'Brien *et al.*, "Integrated Photonic Sensors for Real-Time Label-Free Detection," *ACS Photonics*, vol. 9, pp. 3158–3172, 2022.

[63] A. K. M. Rakib, R. Rahad, M. O. Faruque, and R. H. Sagor, "ZrN-based plasmonic sensor: A promising alternative to traditional noble metal-based sensors for CMOS-compatible and tunable optical properties," *Optics Express*, vol. 31, p. 25280, Jul. 2023.

[64] R. Rahad, A. K. Rakib, M. A. Haque, S. S. Sharar, and R. H. Sagor, "Plasmonic refractive index sensing in the early diagnosis of diabetes, anemia, and cancer: An exploration of biological biomarkers," *Results in Physics*, vol. 49, Jun. 2023.

[65] M. A. Butt, N. L. Kazanskiy, and S. N. Khonina, "Metal–insulator–metal waveguide plasmonic sensor system for refractive index sensing applications," *Advanced Photonics Research*, vol. 4, Jul. 2023.

[66] T. Afdol, M. O. Faruque, R. A. Mahmud, R. H. Sagor, A. K. Nahin, M. A. A. A. Aumi, K. M. Hasan, S. Sazid, and N. M. N. Nasser, "Numerical analysis of an asymmetric hexagonal plasmonic refractive index sensor model based on metal–insulator–metal and Si–insulator–Si waveguide," *Sensing and Bio-Sensing Research*, vol. 40, Jun. 2023.

[67] R. Rahad, A. K. Rakib, M. K. Mahadi, and M. O. Faruque, "Fuel classification and adulteration detection using a highly sensitive plasmonic sensor," *Sensing and Bio-Sensing Research*, vol. 40, Jun. 2023.

[68] S. Rohimah, H. Tian, J. Wang, J. Chen, J. Li, X. Liu, J. Cui, Q. Xu, and Y. Hao, "Fano resonance in the plasmonic structure of MIM waveguide with R-shaped resonator for refractive index sensor," *Plasmonics*, vol. 17, pp. 1681–1689, Aug. 2022.

[69] M. O. Faruque, R. A. Mahmud, and R. H. Sagor, "Highly sensitive plasmonic refractive index sensor using doped silicon: An alternative to MIM structures," *Plasmonics*, vol. 17, pp. 203–211, Feb. 2022.

[70] S. Khani and M. Hayati, "An ultra-high sensitive plasmonic refractive index sensor using an elliptical resonator and MIM waveguide," *Superlattices and Microstructures*, vol. 156, Aug. 2021.

[71] I. Tathfif, K. S. Rashid, A. A. Yaseer, and R. H. Sagor, "Alternative material titanium nitride based refractive index sensor embedded with defects: An emerging solution in sensing arena," *Results in Physics*, vol. 29, Oct. 2021.

[72] K. S. Rashid, M. F. Hassan, A. A. Yaseer, I. Tathfif, and R. H. Sagor, “Gas-sensing and label-free detection of biomaterials employing multiple rings structured plasmonic nanosensor,” *Sensing and Bio-Sensing Research*, vol. 33, Aug. 2021.

[73] R. A. Mahmud, M. O. Faruque, and R. H. Sagor, “Plasmonic refractive index sensor based on ring-type pentagonal resonator with high sensitivity,” *Plasmonics*, vol. 16, pp. 873–880, Jun. 2021.

[74] A. A. Yaseer, M. F. Hassan, I. Tathfif, K. S. Rashid, and R. H. Sagor, “Plasmonic refractive index sensor optimized for color detection,” *Research Square*, preprint, Sep. 2021. [Online]. Available: https://www.researchsquare.com/article/rs-826969/v1

[75] A. Boltasseva and H. A. Atwater, “Alternative plasmonic materials to gold and silver,” *Science*, vol. 331, no. 6015, pp. 290–291, 2011.

[76] P. R. West, S. Ishii, G. V. Naik, N. K. Emani, V. M. Shalaev, and A. Boltasseva, “Searching for better plasmonic materials,” *Laser & Photonics Reviews*, vol. 4, no. 6, pp. 795–808, 2010.

[77] G. V. Naik, V. M. Shalaev, and A. Boltasseva, “Alternative plasmonic materials: Beyond gold and silver,” *Advanced Materials*, vol. 25, no. 24, pp. 3264–3294, 2013.

[78] U. Guler, V. M. Shalaev, and A. Boltasseva, “Plasmonics with titanium nitride: Alternative material for high-temperature applications,” *Optical Materials Express*, vol. 5, no. 11, pp. 2501–2520, 2015.

[79] E. Feigenbaum, K. Diest, and H. A. Atwater, “Plasmonics in heavily doped semiconductors,” *Nano Letters*, vol. 10, no. 6, pp. 2111–2116, 2010.

[80] S. Kim, S. Lee, and J.-H. Park, “Enhanced plasmonic biosensing using dielectric oxides in hybrid nanostructures,” *ACS Photonics*, vol. 5, no. 9, pp. 3703–3710, 2018.

[81] J. Liu, Y. Wang, and Y. Zhang, “High-performance hybrid plasmonic sensors with dielectric oxide layers,” *Scientific Reports*, vol. 6, p. 29245, 2016.

[82] R. Soref, “Mid-infrared photonics in silicon and germanium,” *Nature Photonics*, vol. 4, pp. 495–497, 2010.

[83] A. N. Grigorenko, M. Polini, and K. S. Novoselov, “Graphene plasmonics,” *Nature Photonics*, vol. 6, pp. 749–758, 2012.

[84] D. Rodrigo, O. Limaj, D. Janner, D. Etezadi, F. J. García de Abajo, V. Pruneri, and H. Altug, “Mid-infrared plasmonic biosensing with graphene,” *Science*, vol. 349, no. 6244, pp. 165–168, 2015.

[85] C. F. Bohren and D. R. Huffman, *Absorption and Scattering of Light by Small Particles.* John Wiley & Sons, Ltd, 1998.

[86] A. Moroz, "Three-dimensional complete photonic-band-gap structures in the visible," *Physical Review Letters*, vol. 83, pp. 5274–5277, Dec. 1999.

[87] C. S. H. Hwang, M. S. Ahn, and K. H. Jeong, "Extraordinary sensitivity enhancement of Ag–Au alloy nanohole arrays for label-free detection of *Escherichia coli*," *Biomedical Optics Express*, vol. 12, no. 5, pp. 2734–2743, Apr. 2021. Published online Apr. 15, 2021.

[88] C. Gao, Y. Hu, M. Wang, M. Chi, and Y. Yin, "Fully alloyed Ag/Au nanospheres: Combining the plasmonic property of Ag with the stability of Au," *Journal of the American Chemical Society*, vol. 136, no. 20, pp. 7474–7479, 2014. PMID: 24821567.

[89] R. K. Roy, S. K. Mandal, and A. K. Pal, "Effect of interfacial alloying on the surface plasmon resonance of nanocrystalline Au–Ag multilayer thin films," *The European Physical Journal B – Condensed Matter and Complex Systems*, vol. 33, no. 1, pp. 109–114, 2003.

[90] D. T. N. Anh, P. Singh, C. Shankar, D. Mott, and S. Maenosono, "Charge-transfer-induced suppression of galvanic replacement and synthesis of (Au@Ag)@Au double-shell nanoparticles for highly uniform, robust, and sensitive bioprobes," *Applied Physics Letters*, vol. 99, no. 7, 2011.

[91] İ. Candan, "Investigation of plasmonic Ag–Au alloy nanoparticles," *International Journal of Health and Applied Science*, vol. 1, no. 1, pp. 14–23, 2023.

[92] V. R. Manikam, K. Y. Cheong, and K. A. Razak, "Chemical reduction methods for synthesizing Ag and Al nanoparticles and their respective nanoalloys," *Materials Science and Engineering: B*, vol. 176, no. 3, pp. 187–203, 2011.

[93] V. Coviello, D. Forrer, and V. Amendola, "Recent developments in plasmonic alloy nanoparticles: Synthesis, modelling, properties, and applications," *ChemPhysChem*, vol. 23, no. 21, e202200136, 2022.

[94] D. Rioux, S. Vallières, S. Besner, P. Muñoz, E. Mazur, and M. Meunier, "An analytic model for the dielectric function of Au, Ag, and their alloys," *Advanced Optical Materials*, vol. 2, no. 2, pp. 176–182, 2014.

[95] Oduncuoğlu, M., "Refractive Index Formula of Blood as a Function of Temperature and Concentration," *Anais da Academia Brasileira de Ciências*, vol. 93, suppl. 4, e20201634 (2021).

[96] M. Salaheldeen, A. Satti, and B. Awadallah, "Storage and thermal behavior of some cooking oils consumed from the local market of Sudan," *Sudanese Journal of Science*, vol. 7, pp. 919–924, July 2019.

[97] O. Zhernovaya, O. Sydoruk, V. Tuchin, and A. Douplik, "The refractive index of human hemoglobin in the visible range," *Physics in Medicine and Biology*, vol. 56, pp. 4013–4021, July 2011. doi:10.1088/0031-9155/56/13/017

15% Overall Similarity

The combined total of all matches, including overlapping sources, for each database.

Filtered from the Report

- Bibliography

Match Groups

- **220 Not Cited or Quoted 14%**
  Matches with neither in-text citation nor quotation marks
- **3 Missing Quotations 1%**
  Matches that are still very similar to source material
- **0 Missing Citation 0%**
  Matches that have quotation marks, but no in-text citation
- **0 Cited and Quoted 0%**
  Matches with in-text citation present, but no quotation marks

Top Sources

9%	Internet sources
12%	Publications
4%	Submitted works (Student Papers)

Mohammad Ashfaqur Rahman Asif

Fatema Tasnim Oyshi Fatema Tasnim

Safwan Sami Safwan

20/10/25

Prof. Dr. Rakibul Hasan Sagor